

BIOLUMINESCENCE IN THE ARCTIC POLAR NIGHT

by

Heather A. Cronin

A thesis submitted to the Faculty of the University of Delaware in partial fulfillment of the requirements for the degree of Master of Science in Marine Studies

Summer 2015

© 2015 Heather A. Cronin
All Rights Reserved

ProQuest Number: 1602340

All rights reserved

INFORMATION TO ALL USERS

The quality of this reproduction is dependent upon the quality of the copy submitted.

In the unlikely event that the author did not send a complete manuscript and there are missing pages, these will be noted. Also, if material had to be removed, a note will indicate the deletion.



ProQuest 1602340

Published by ProQuest LLC (2015). Copyright of the Dissertation is held by the Author.

All rights reserved.

This work is protected against unauthorized copying under Title 17, United States Code
Microform Edition © ProQuest LLC.

ProQuest LLC.
789 East Eisenhower Parkway
P.O. Box 1346
Ann Arbor, MI 48106 - 1346

BIOLUMINESCENCE IN THE ARCTIC POLAR NIGHT

by

Heather Cronin

Approved: _____
Jonathan H. Cohen, Ph.D.
Professor in charge of thesis on behalf of the Advisory Committee

Approved: _____
Mark A. Moline, Ph.D.
Director of the School of Marine Science and Policy

Approved: _____
Nancy M. Targett, Ph.D.
Dean of the College of Earth Ocean and Environment

Approved: _____
James G. Richards, Ph.D.
Vice Provost for Graduate and Professional Education

ACKNOWLEDGMENTS

First and foremost, I must thank my two excellent advisors, Dr. Jonathan Cohen and Dr. Mark Moline, without whose guidance this project would not have been possible. I thank you both for your incredible patience, for pushing me to achieve more and produce a better product at every step along the way, and for giving me the opportunity to tackle this project. Also, thank-you for traveling to the far reaches of the world with me and for introducing me to Svalbard, where you had my back against polar bears, and to which you sent me back for a solo-mission. You've not only helped me to become better as an academic and a scientist, but also introduced me to an international family of marine scientists who will be an incredible resource in my future. I must also thank my final committee member, Dr. Doug Miller, for his generous guidance and the new perspectives that he brought to my work. I thank Dr. Jørgen Berge and Dr. Geir Johnsen for their collaboration on this project, for their roles as leading instructors during courses at UNIS, and for their boundless humor which kept us all laughing during 5 weeks of darkness.

Marcia Pettay has been an integral resource to me throughout my master's work, and so I thank her for her assistance in planning my travel, managing my advisors, and helping me maintain my sanity. The members of the Cohen Lab, Adam Wickline and Corie Charpentier have been incredible friends and role models. From taking cruises in the Delaware Bay, to measuring eels in the marsh, and to endless hours in dark rooms or wading through MatLab-I am so thankful for our tight knit group. My family, of course, has been full of encouragement, love, and support

throughout these past two years, and I thank them all for always believing in me. I must finally acknowledge the exceptionally supportive community of students and faculty that we have here at the University of Delaware, and extend the greatest warmth and gratitude to the members of the UNIS AB 320 and AB 334 courses.

TABLE OF CONTENTS

LIST OF TABLES	vii
LIST OF FIGURES	viii
ABSTRACT	x
Chapter	
1 GENERAL INTRODUCTION	1
2 WINTER COMPOSITION AND DISTRIBUTION OF ARCTIC BIOLUMINESCENT COMMUNITIES: IMPLICATIONS FOR TROPHIC INTERACTIONS.....	5
2.1 Introduction	5
2.2 Methods	8
2.2.1 Field Measurements.....	9
2.2.1.1 Bioluminescence.....	9
2.2.1.2 Optical Properties and Diffuse Irradiance ..	10
2.2.2 Laboratory Measurements	11
2.2.2.1 Flash-kinetic Library	11
2.2.2.2 Visual physiology of <i>T. inermis</i>	14
2.2.3 Visual Modeling	14
2.3 Results	16
2.3.1 Physical properties and the underwater light field	16
2.3.2 Bioluminescence in Kongsfjord	17
2.3.3 Modeling the visual range of <i>Thysanoessa inermis</i>	19
2.4 Discussion.....	20
REFERENCES	37

Appendix

A	DEVELOPMENT OF <i>IN SITU</i> IDENTIFICATION METHOD.....	44
B	VISUAL MODELS	47
B.1	Model Parameters	47
B.1.1	<i>Thysanoessa inermis</i> eye morphology.....	48
B.1.2	<i>Thysanoessa inermis</i> eye physiology	49
B.1.3	Underwater Light Field in Kongsfjord	50
B.2	ADDITIONAL MODEL RESULTS.....	51

LIST OF TABLES

Table 2.1: Flash kinetic parameter signatures (\pm SE) for taxa collected around Svalbard during 2012 and 2014. Sample size is in parentheses with each taxon. BL_{\max} , BL_{mean} , and \sum_{\max} are reported $\times 10^9$ photons s^{-1} , and T_{\max} is reported in seconds.....	29
Table 2.2: Mean abundances (individuals m^{-3} , \pm SE) of each taxon in the bioluminescence library for UBAT profiles (n=4) shown in Fig. 2.4. Abundances are calculated from the first 4 minutes (89.5 L) sampled. ..	30
Table 2.3: Maximum Shannon diversity (H'_{\max}) and the time (s) to reach $\frac{1}{2}$ of the maximum diversity (K) calculated from non-linear regression of Shannon diversity at every 30s during UBAT profiles (Fig. 2.6), and mean measured Shannon diversity (H') and Pielou's evenness (J') for the entire sampling period.	35
Table A.1: Mean cumulative error (Φ) and standard deviation of that error ($\sigma\Phi$) used to create a taxon-specific threshold value for $\bar{\varphi}$, the cumulative error between an <i>in situ</i> emission and a taxonomic signature.....	46
Table A.2: Percentage of correct identifications for each taxon tested in the laboratory, using different sequences of iterative identification. “% within threshold” represents the percentage of individuals from the laboratory dataset with a $\bar{\varphi}$ which fell within the identification threshold, and were able to be identified using this method. Order 1 was used for <i>in situ</i> identifications in Kongsfjord.....	46
Table B.1: A list of component equations for visual models of the detection of an extended black target triggering bioluminescence and a description of their purposes. All equations are from Nilsson et al. (2014). Variable definitions and their values are listed in Table B.3.	54
Table B.2: Taxon-specific E-values for each of the seven taxa in the bioluminescence library.	54
Table B.3: Variables used in visual models and their values. Variables are from Nilsson et al. (2014); ρ is for calculations of nearest neighbor distances from Clark and Evans 1979 (see above).....	55

LIST OF FIGURES

- Figure 2.1: Flash kinetics for an emission from a laboratory-tested copepod *Metridia longa* showing parameters used to create taxonomic signatures for *in situ* identifications. Parameters include the maximum bioluminescence (BL_{max}), the average bioluminescence produced during the emission (BL_{mean}), the time until the emission reached maximum (T_{max}), and the cumulative sum of bioluminescence produced until the maximum (Σ_{max}). 28
- Figure 2.2: (A) Mean profiles (n=3) of salinity, temperature and σ_{θ} ($\pm SE$) taken by CTD (2014) concurrent with measurements of bioluminescence potential. (B) Downwelling spectral irradiance modelled in Kongsfjord for midday on 25 January 2015 as described in Methods (Section 2.2). 31
- Figure 2.3: Distribution of photons from biological and atmospheric light sources as a function of depth in January in Kongsfjord. Photons from mean bioluminescence potential ($\pm SE$, black dots) measured at midday and midnight, and scalar irradiance between 400-700nm (E_0, PAR , solid line) modeled from diffuse atmospheric irradiance measured at approximately solar noon on 25 January 2015. 32
- Figure 2.4 Bioluminescence profiles. (A) Profiles of mean bioluminescence potential ($\pm SE$, n=4) measured for 4 minutes at 20 m intervals. Profiles were taken in Kongsfjord (2014). Bioluminescence potential is represented as total number of emissions m^{-3} (dark bars) and in number of photons ($\times 10^{13} m^{-3}$) produced (light bars). (B-G) Proportion of the bioluminescent community (as measured by number of emissions) comprised by each known bioluminescent taxonomic group and by unidentified individuals. Compound flashes which were not processed using the bioluminescence library are also included. 33
- Figure 2.5: Multidimensional scaling of bioluminescent communities based on abundances (individuals m^{-3}) of 7 taxonomic groups (Table 2.2) for samples (n=4) at 20m depth intervals in UBAT profiles. Taxonomic abundances are square-root transformed and resemblance is plotted according to Bray-Curtis dissimilarity. 34

Figure 2.6: Mean (n=4) Shannon diversity at every 30s for each depth interval over the 4-minute (89.5 L) sampling period for profiles in Figure 2.4. Overlaid, is a nonlinear regression model for each depth. Grey symbols/lines represent communities at 60m and below, while dark symbols/lines represent communities at 40m and above. 35

Figure 2.7 Visual range of an upward-looking *T. inermis* observing an approaching little auk (*Alle alle*) in light conditions shown in Figure 2.2B. (A) Visual range given the bioluminescent community determined from UBAT profiles in January 2014 (solid line) compared to no bioluminescence (dotted line). The shaded box represents the range (0.76m) within which the little auk subtended greater than 28° of the visual field of *T. inermis*. In this range, photoreceptors in the *T. inermis* eye could not simultaneously view both the little auk and the background, and therefore *T. inermis* could not discriminate the little auk. (B) Visual range given bioluminescence from single populations of each of the three most abundant taxonomic groups in Kongsfjord. Gray dashed lines in both panels represent depths at which the input community for the model was altered to reflect the community in Kongsfjord. 36

Figure B.1: Sagittal section of a *T. inermis* eye showing focal length, f , and photoreceptor diameter, d . This individual was collected in Kongsfjord during January 2015. 53

Figure B.2: Visual range of *T. inermis*, found using theoretical values of nearest neighbor distance and point source emissions for common taxonomic groups in Kongsfjord. 56

ABSTRACT

In the featureless pelagic environment, the submarine light field plays an important role in structuring population dynamics by influencing a variety of biological processes and trophic interactions. For many marine organisms, bioluminescence is the main visual stimulus as downwelling atmospheric light attenuates with depth. However, the distribution of bioluminescent plankton is variable with depth, and bioluminescent species differ in the intensity of their emissions, causing the bioluminescent light field to be dependent on the composition and distribution of the bioluminescent community. Mechanically-stimulated bioluminescence, or bioluminescence potential, interacts with background ambient light to influence light-mediated behaviors, such as visual search for predators or prey, thus having a potentially large influence on ecosystem dynamics and function through trophic interactions. Nevertheless, bioluminescent community dynamics and the role of bioluminescence in larger ecosystem function remain to be characterized for many systems.

In order to understand the ecological role of bioluminescence in dim environments this study investigated winter bioluminescent communities in Kongsfjord, Svalbard, a high Arctic fjord (78°N, 55°E), during January 2014. Kongsfjord during this time of the year experiences low atmospheric irradiance for an extended period, due to the sun being below the horizon for the duration of the polar night. Therefore, the amount of light available for visually-mediated behaviors and trophic interactions in the pelagic zone is also dim. However, bioluminescence occurs

throughout the water column, and some overwintering visual predators in Kongsfjord have been shown to feed on bioluminescent taxa. Therefore, Kongsfjord represents a unique environment for investigating shallow water bioluminescent communities and the trophic role of bioluminescence within these communities. With this study, I report the depth distribution and taxonomic composition of bioluminescent plankton as determined by a profiled bathyphotometer in Kongsfjord, and create a pelagic photon budget for atmosphere-derived scalar irradiance and bioluminescence potential. To explore the potential for bioluminescence to affect food-web dynamics in Kongsfjord, I also model the influence of bioluminescent light fields from measured communities on a relevant visual trophic interaction.

The 20m to 40m depth range in Kongsfjord represented a transition zone in which taxonomic abundance, diversity indices, and bioluminescence potential indicated shallow and deep bioluminescent communities. Bioluminescence potential in the water column peaked at 80m, and dinoflagellates were the most abundant taxonomic group at or above 20m, while the copepod *Metridia longa* was the most abundant taxon below 20m. By quantifying the visual sensitivities of a key micronekton, the euphausiid *Thysanoessa inermis*, community-generated bioluminescent light fields measured in Kongsfjord were applied to a visual model for krill viewing one of its winter predators, the little auk (*Alle alle*). Depending on the depth of *T. inermis*, and therefore the intensity of background space-light, emissions from bioluminescent communities in Kongsfjord either illuminated or camouflaged the diving little auk. This study also determined that the number of photons contributed to the pelagic photon budget by bioluminescence in Kongsfjord surpassed atmosphere-derived scalar irradiance between 20 and 40m. At depths as shallow as

60m, bioluminescence contributes 98% or more of pelagic photons, indicating that during winter in Kongsfjord, bioluminescence plays a disproportionate role in predator-prey dynamics during the day than in other shallow daytime ecosystems.

Chapter 1

GENERAL INTRODUCTION

Bioluminescence, or the chemical generation of visible light by an organism (Haddock et al. 2010, Widder 2010), is a pervasive phenomenon in the world's oceans. Used by 16 different phyla (Herring 1987, Haddock et al. 2010), bioluminescence may be observed from the tropics to the poles and from surface to deep waters and benthic habitats (e.g. Haddock and Case 1999, Heger 2008, Johnsen et al. 2012). Generally, bioluminescence is produced via an oxidation-reduction reaction involving a luciferin protein and a luciferase or photoprotein catalyst (Wilson and Hastings 1998). This light-generating reaction has potential use for a number of different ecological interactions, including “defensive” strategies, “offensive” strategies, and interspecific communication (reviewed by Haddock et al. 2010).

In environments which experience diel light-dark cycles, darkness is a resource which is necessary to some species for successful growth and reproduction, and the effectiveness of bioluminescence is dependent on a lower limit of atmospheric illumination (Gerrish et al. 2009). Hence, dinoflagellates, which use “burglar alarm” emissions to illuminate their predators to secondary predators (Messinger and Case 1992), have developed a circadian rhythm of bioluminescence, experiencing photoinhibition of bioluminescence at daytime light levels (e.g. Sullivan and Swift 1994; Li et al. 1996). Other organisms, such as cypridinid ostracods, exhibit complex bioluminescent signals for mate attraction after the sun sets (Rivers and Morin 2008), using low levels of atmospheric irradiance as an opportunity for luminescent courtship

displays. Furthermore, species, such as the copepod *Metridia* spp., which migrate to shallow waters at night to feed (Hays 1995), may use bioluminescence as a deterrent for nocturnal predation or to communicate between conspecifics during predatory attacks (Buskey and Swift 1985).

Downwelling atmospheric light decreases exponentially with depth (Smith et al. 1989) and space-light comes increasingly from above in deeper environments (Warrant 2004). Due to changes in the light field with increasing depth, changes in visual predator-prey interactions may drive organism physiology (Childress et al. 1990). The visual interactions hypothesis (Childress et al. 1990) states that the evolution of lower metabolic rates and locomotor abilities in deeper-living pelagic fishes and crustaceans is due, in part, to the decline in the distances over which predator and prey can visually detect each other due to decreasing light intensity. Bioluminescence, however, may affect visual range in these environments as it increases in relative intensity to other light sources in deeper waters (Smith et al. 1989). Therefore, the composition and distribution of bioluminescence may play a central role in the amount light available for visually-mediated trophic interactions.

Many mesopelagic and deep-sea organisms have wide pupils, as well as good spatial resolution for viewing bioluminescent point sources (Warrant and Locket 2004). In these environments, some organisms use bioluminescent lures to attract prey (Haddock et al. 2005) or photophores to illuminate prey (Partridge and Douglas 1995) and diving species use stimulated bioluminescence to find or attract prey (Vacquié-Garcia et al. 2012). Finally, deep living prey species may use sacrificial luminescent tags (Herring and Widder 2004), bioluminescent “smoke screens” (Robison et al. 2003), or burglar alarm emissions to deter predators (Robison 1992). However, despite

this bioluminescence “arms-race” between predators and prey (Dawkins and Krebs 1979), the quantitative impact of bioluminescence on trophic interactions remains unclear. Additionally, unlike other biological characteristics which can act as indicators of the functional state of marine ecosystem (e.g. phytoplankton and zooplankton biomass or chlorophyll-*a* concentration) (Piontkovski et al. 1997), bioluminescence, measured for the community, has been understudied in terms of distribution patterns and ecosystem functionality (e.g. Batchelder et al. 1990; Moline et al. 2009).

By investigating the effect of bioluminescent light fields on vision, the impact of bioluminescent communities for trophic interactions in otherwise dark environments, and therefore their role in ecosystem function, may be better understood. To do this, the Arctic winter provides a unique model ecosystem. During the Arctic winter the polar night occurs when the sun does not rise above the horizon for a minimum of 24 hours, with the period of time and the degree to which the sun is below the horizon increasing at higher latitudes (Berge et al. In Press.). As a result, in the high Arctic (above 78° N), a seasonal photoperiod occurs rather than a more typical diel photoperiod experienced in more southern climates. For an extended period of time, organisms living in shallow waters during the polar winter experience low levels of irradiance which has the potential to affect both behaviors that are dependent on light cues (e.g. DVM; Båtnes 2013) or visually mediated trophic interactions in shallow waters.

In Kongsfjord, Svalbard (78 °N, 55°E) the polar night, lasts for 129 days (Berge et al. In Press.). Atmospheric light at this time approaches the perception limits of local zooplankton at depths as shallow as 30m (Cohen et al. 2015). In such a light

regime, bioluminescence in shallow waters may play an important role for visually mediated trophic interactions. Zooplankton communities around Svalbard are relatively dilute and are dominated by a few species (Dvoretzky and Dvoretzky 2014), and in Svalbard fjords winter communities decrease both in biomass and in number of taxa (Weslawski et al. 1991). However, although communities may be more dilute, bioluminescence occurs throughout the water column during the polar night in Kongsfjord (Berge et al. 2012), with some bioluminescent species becoming more common around Svalbard in winter than in summer (Weslawski et al. 1991). Low planktonic diversity and density during this portion of the year create a relatively simple system for studying the community dynamics and distribution of bioluminescent plankton. In addition, because some overwintering visual predators have shown a preference for bioluminescent taxa (Berge et al. In Prep.), Kongsfjord may be an ideal system for investigating the ecological role of bioluminescence in shallow environments that experience extended periods of darkness.

Therefore, in order to begin to understand the role of bioluminescence for trophic dynamics and larger ecosystem function in dim environments, this study seeks to answer the questions:

1. What is the spatial structure and community composition of bioluminescent planktonic organisms in Kongsfjord at this time of the year?
2. Could bioluminescence produced by this planktonic community affect light-mediated trophic interactions during the Arctic polar night?

Chapter 2

WINTER COMPOSITION AND DISTRIBUTION OF ARCTIC BIOLUMINESCENT COMMUNITIES: IMPLICATIONS FOR TROPHIC INTERACTIONS

2.1 Introduction

Interactions between organisms in the pelagic realm are largely mediated by vision (Johnsen et al. 2001, Widder 2002), and species may employ cryptic strategies such as transparency (e.g. Zylinski and Johnsen 2011) counterillumination (e.g. Jones and Nishiguchi 2004), and diel vertical migration (Lampert 1993) to remain hidden from potential predators (Widder et al. 1999, Johnsen 2014). As a result, the underwater light field impacts the distribution and behavior of pelagic organisms due, in part, to its influence on trophic interactions. Bioluminescence, or the natural chemical generation of light by an organism (Haddock et al. 2010; Widder 2010), provides an additional source of light in pelagic environments to supplement those photons derived from the atmosphere. By illuminating swimming organisms, bioluminescence can enhance the ability of prey to detect potential predators at sufficient distances to apply an appropriate behavioral response (e.g. Nilsson et al. 2012). Therefore, describing the distribution of bioluminescence and its contribution to the pelagic light field is key to understanding the distribution and behavior of visual predators and their prey.

At a given depth, the contribution of bioluminescence to the pelagic light field is dependent on the distribution of bioluminescent organisms and the intensity of the

bioluminescence they produce (e.g. Batchelder et al. 1992), as well as the intensity of atmosphere-derived light (Smith et al. 1989). Since larger bioluminescent nekton are sparsely distributed in the upper 1000m of the water column (Buskey 1992), the bioluminescent light field is dependent on the density and distribution of bioluminescent plankton, which can be patchy or aggregated in thin layers throughout the water column (Kushnir et al. 1997; Widder et al. 1999, Cussatlegras et al. 2001). Thus, *in situ* bioluminescence measurements have been used to investigate the taxonomic composition and 3-dimensional distribution of bioluminescent assemblages using a variety of techniques; including the spatial plankton analysis technique (SPLAT) (e.g. Widder and Johnsen 2000), and bioluminescence budget analysis, which uses a combination of bathyphotometer measurements and net sampling to develop a light budget for each luminescent species (e.g. Lapota et al. 1992). Bathyphotometers, which measure mechanically-stimulated bioluminescence, consist of an enclosed chamber with a photomultiplier tube through which turbulent flow draws in and stimulates organisms to luminesce (Latz and Rohr 2013). The radiant energy emitted by organisms in response to this stimulus is termed *bioluminescence potential* (Widder et al. 1993). In coastal environments, bioluminescence potential measured by small-volume bathyphotometers can provide fine-scale resolution of populations of small zooplankton and dinoflagellates based on emission intensity and flash kinetics (Herren et al. 2005, Moline et al. 2009, Johnsen et al. 2014).

In the Arctic, bioluminescence is found throughout the planktonic food web, from primary producers such as the dinoflagellate *Ceratium* spp. through secondary consumers, e.g. *Meganyctiphanes norvegica* or *Thysanoessa* spp. (Herring 1987). During spring, summer and autumn, the distribution and composition of

bioluminescence in the Arctic has been investigated using a combination of net sampling and bathyphotometer profiling in fjords, open water, and beneath sea ice. In marginal ice zones larger mesozooplankton and micronekton contribute the majority of bioluminescence (Buskey 1992), with dinoflagellate-dominated surface bioluminescence shifting to copepod luminescence in deeper waters (Lapota et al. 1992). However, in coastal fjords, dinoflagellates dominate the bioluminescence budget with copepods contributing very little (Lapota et al. 1989), and under sea ice bioluminescent plankton aggregate in thin layers (Gitel'zon et al. 1981).

The only studies of bioluminescence in the Arctic winter have been conducted recently, where bioluminescence was investigated using flash kinetics in a bathyphotometer in Kongsfjord, Svalbard (Berge et al. 2012; Johnsen et al. 2014). At this time of the year, an understanding of the taxonomic composition and depth distribution of bioluminescent planktonic communities is limited to a shallow 51-hour time series (Johnsen et al. 2014) and horizontal transects at 15, 45 and 75m (Berge et al. 2012). Active predation continues through the polar winter at this location (Berge et al. 2012; Kraft et al. 2012), despite low levels of ambient daylight as the sun remains below the horizon (Cohen et al. 2015). Due to this low ambient light, bioluminescence may contribute a proportionally higher number of photons than atmospheric light to the pelagic light budget in Kongsfjord (see Smith et al. 1989), and therefore bioluminescent communities are likely to have a greater influence on predator-prey dynamics in Kongsfjord during winter than at other times of the year. Thus, characterizing bioluminescent plankton communities is the first step to understanding visually-mediated trophic interactions in Kongsfjord during the Arctic winter.

This study first seeks to understand the depth distribution of bioluminescence potential in Kongsfjord during the Arctic winter, and to describe the planktonic community that contributes to pelagic bioluminescence using flash kinetics to identify taxa. Further, I examine the relative contribution of measured bioluminescence potential to the pelagic light budget by modeling atmosphere-derived light in Kongsfjord. Finally, I investigate the interaction between a dominant micronekton species, the euphausiid *Thysanoessa inermis*, and one of its winter predators, the little auk *Alle alle*, by modeling the visual range of *T. inermis* in the context of the bioluminescent light field created by measured communities.

2.2 Methods

In order to examine bioluminescence potential and the depth distribution and community composition of bioluminescent plankton in Kongsfjord, *in situ* bioluminescent emissions in a profiled Underwater Bioluminescence Assessment Tool (UBAT; WetLabs, Inc., Philomath, OR) were identified using a library of flash kinetic signatures developed through testing individuals with this instrument in the laboratory. The relative contribution of bioluminescence to the pelagic light field in Kongsfjord was determined by creating a photon budget from modeled scalar irradiance and measured bioluminescence potential. To evaluate the effect of bioluminescence from measured communities on a relevant winter trophic interaction, the visual range for *Thysanoessa inermis* viewing a little auk (*Alle alle*) was also modeled. Visual models for *T. inermis* under conditions in Kongsfjord required input for background space-light and inherent optical properties, and were tailored to *T. inermis* living in Kongsfjord during winter by using measurements of visual structures and electrophysiology of *T. inermis* in January 2014 and 2015 to parameterize the model.

Therefore, methods are divided into three sections with subheadings: Field Measurements (bioluminescence profiles, *in situ* optical properties and irradiance measurements used for input to a radiative transfer model), Laboratory Measurements (development of the flash kinetic library and physiological and morphological measurements of *T. inermis*), and Visual Modeling.

2.2.1 Field Measurements

2.2.1.1 Bioluminescence

Four bioluminescence and CTD profiles (SBE 49 FastCAT, Sea-Bird, Bellevue, WA), two at midday and two at midnight, were taken using an Underwater Bioluminescence Assessment Tool (UBAT) between 21 and 24 January, 2014 at 78.936°N, 11.943°E. Profiles were taken from the surface to 120m (bottom depth≈ 200m) and were stopped for four minutes at every 20m to measure the bioluminescent community (Smith et al. 1989, Buskey 1992). Stop lengths were determined from an analysis of the variation in bioluminescence potential, or the radiant energy produced by an organism in the UBAT in response to the turbulent stimulus, during a preliminary UBAT deployment at static depth. The total number of emissions measured by the UBAT represented the number of bioluminescent individuals sampled. For each depth interval, a ratio of bioluminescence potential to number of bioluminescent emissions was developed and compared across depth intervals using a Kruskal-Wallis test. Organisms responsible for producing each luminescent flash in the UBAT record were identified using a library of taxon-specific signatures developed in the laboratory (see section 2.2.2.1).

Taxonomic abundances were calculated from the number of individuals identified as each of the seven taxa in the bioluminescence library and the volume of water pumped by the UBAT during each stop, 89.5 L. To assess the effect of local time on bioluminescence measurements the abundance of individual taxa (Two-way ANOVA, $P > 0.05$), the total number of individuals sampled (Two Way ANOVA, $F(14, 27) = 0.786$, $P = 0.6$), and the total bioluminescence potential (Two-way ANOVA, $F(14, 27) = 1.639$, $P = 0.2$) were tested for significant differences between samples taken at midday and at midnight at any depth. Accordingly, all four casts were considered replicates for future analyses. To quantify differences in community structure at depth intervals, Shannon diversity (Shannon 1948) and Pielou's evenness (Pielou 1966) indices were calculated for each 4 minute sample. For every replicate, Shannon diversity was also calculated at 30s intervals during the sampling period and replicates for each depth interval were fit with a nonlinear regression model based on a Michaelis-Menten function. The maximum diversity, H'_{\max} , and the time to half-maximum diversity, K , were calculated from the regression for each depth. To visualize differences in community structure, taxonomic abundances for each replicate at each depth were plotted using multi-dimensional scaling (MDS). Abundances for MDS were square-root transformed to de-emphasize taxa with high abundances and communities were plotted according to Bray-Curtis dissimilarity (Bray and Curtis 1957).

2.2.1.2 Optical Properties and Diffuse Irradiance

In order to investigate the relative contribution of bioluminescent potential to the pelagic light field and to develop a photon budget for the water column in Kongsfjord, inherent optical properties in Kongsfjord, measured via an AC-9

(WetLabs, Inc., Philomath, OR) profile and diffuse skylight were measured in January 2015. Additionally, visual range was dependent on internal (bioluminescent) and external (atmosphere-derived) light at the position of *T. inermis* in the water column, so inherent optical properties in Kongsfjord and diffuse skylight were also used to parameterize visual models. Briefly, atmospheric light measured on 25 January 2015 [see Cohen et al. (2015) for measurement detail] was input to Hydrolight 5.2 RTE model (Mobley & Sundman 2001) as spectral irradiance, and downwelling radiance in Kongsfjord was modeled from 390 to 700 nm for clear sky conditions with the inclusion of Raman scattering and chlorophyll-*a* fluorescence, as described in Cohen et al. (2015) and Appendix B. Scalar irradiance modeled at every meter was used for photon budgets (see Smith et al. 1989), while background space-light for input into visual models was determined at every meter by weighting the downwelling radiance spectrum at each depth by the spectral sensitivity of *T. inermis* found via electroretinography in January 2014 (Cohen et al. 2015; Appendix B), and integrating across wavelengths.

2.2.2 Laboratory Measurements

2.2.2.1 Flash-kinetic Library

Bioluminescent emissions measured *in situ* were compared to a library of taxon-specific bioluminescence flash kinetics developed in the laboratory to determine the composition and vertical distribution of the Kongsfjord bioluminescent community. This library was developed in 2014 by testing plankton collected from three Svalbard fjords (Kongsfjord, Rijpfjord, and Billefjord), and once sea ice station (80.37°N, 11.31°E), for mechanically stimulated bioluminescence in a UBAT under

controlled laboratory conditions. Plankton, sorted by taxon, were inserted into the inflow of the UBAT one individual at a time for larger zooplankton and in groups of multiple individuals for smaller zooplankton and phytoplankton in order to measure the kinetics of their emissions. Since krill were often not stimulated by the turbulence of the UBAT alone, they were gently squeezed with forceps until bioluminescence began prior to being inserted into the inflow. Taxa tested for UBAT-induced bioluminescence included: amphipods (*Themisto abyssorum*, *Themisto libellula*), appendicularians, chaetognaths (*Parasagitta elegans*), cnidarians (*Aglantha digitale*), ctenophores (*Beroe cucumis*, *Mertensia ovum*) copepods (*Calanus* spp., *Metridia longa*, *Oithona* spp., *Paraeuchaeta* spp., *Triconia* spp.), dinoflagellates, krill (*Meganyctiphanes norvegica*, *Thysanoessa inermis*), and ostracods (*Boroecia* spp.). Additionally, existing UBAT measurements were obtained from Johnsen et al. (2014) who used a similar laboratory approach, which augmented the datasets for *Beroe cucumis*, *Metridia longa*, and *Meganyctiphanes norvegica*. Taxa with signatures developed from individuals tested by Johnsen et al. (2014) and in the current study did not differ significantly on any parameter (t-test, $p > 0.05$ for all comparisons) between sampling years.

For taxa which consistently produced bioluminescence in the UBAT, flash kinetics were analyzed to develop a 4-parameter signature, based on methods developed by Johnsen et al. (2014). These parameters were: the maximum bioluminescence produced at any point during the emission (BL_{\max} , photons s^{-1}), the cumulative sum of bioluminescence until the maximum (Σ_{\max} , photons s^{-1}), the time until the emission reached maximum (T_{\max} , s), and the average bioluminescence produced during the emission (BL_{mean} , photons s^{-1}) (Fig. 2.1). To identify the organism

responsible for producing *in situ* emissions measured in Section 2.2.1.1, an error was determined between each emission measured during the first four minutes at profile stops and each taxon-specific signature in the library. This error was calculated as the mean of the individual errors for each of the four flash kinetic parameters [BL_{\max} , BL_{mean} , T_{\max} , and Σ_{\max} ; see Appendix A and Johnsen et al. (2014) for details on error calculations].

In situ emissions were compared to taxonomic signatures in the bioluminescence library iteratively: first to the *Beroe cucumis* signature, and then to *Boroecia* spp., *Metridia longa*, *Mertensia ovum*, *Thysanoessa* spp., *Meganycitiphanes norvegica*, and dinoflagellates respectively. This iterative method was chosen over identifying an emission as the taxon for which it had the smallest error, as done by Johnsen et al. (2014), because it produced the highest number of correct identifications during preliminary analysis of a dataset for which species were known (Appendix A). Emissions were classified as a taxon if the error for that taxon was within one standard deviation of the average error found during analysis of the known dataset (see Appendix A for more on identification method development). Emissions that could not be classified as any taxon in the library were labelled as unidentified, but may consist of bioluminescent appendicularian species (Berge et al. 2012) which were not included in the bioluminescence library. Only emissions which had a BL_{\max} greater than 3×10^8 photons (two orders of magnitude greater than background seawater) and which were not compound were identified. Compound emissions were defined as those with multiple peaks and a minimum between peaks that was either below BL_{mean} or one half an order of magnitude less than BL_{\max} , and were not considered because a true BL_{\max} could not be determined.

2.2.2.2 Visual physiology of *T. inermis*

To parameterize visual range models for the eye of the euphausiid *T. inermis*, aspects of its eye structure (focal length, rhabdom diameter) and physiology (spectral sensitivity, and critical flicker fusion frequency) were measured during January 2014 and 2015. Focal length and rhabdom diameter were measured on semi-thin sections from *T. inermis* eyes, while spectral sensitivity (Cohen et al. 2015) and critical flicker fusion frequency (J. Cohen unpubl. data) were determined via electroretinogram recording. Appendix B provides a detailed description of these morphological and electrophysiological measurements.

2.2.3 Visual Modeling

In order to relate the bioluminescence produced by communities determined above to pelagic trophic interactions, the maximum range at which an abundant micronekton, *Thysanoessa inermis*, could detect a predatory little auk, *Alle alle*, was modeled for the upper 99m of the water column. Calculations were based on those detailed by Nilsson et al. (2014) for discrimination of an extended black target triggering bioluminescence from the ambient background-in this case, the body of a diving little auk stimulating measured bioluminescent communities in Kongsfjord with its wake. The visual range of *T. inermis* was dependent on bioluminescence, downwelling spectrally-weighted radiance, and inherent and apparent optical properties at the position of *T. inermis* the water column, as well as *T. inermis* visual physiology measured in the current study. Range was determined using generalized reduced gradient (GRG) nonlinear optimization of the following equation:

Eq. 2.1

$$|N_{\text{bio}} + N_{\text{black}} + N_{\text{space}}| = R \sqrt{N_{\text{bio}} + N_{\text{black}} + N_{\text{space}} + 2X_{\text{ch}}}$$

(Nilsson et al. 2014; Equation 2.19)

where N_{bio} is the mean photon count originating from bioluminescent sources, N_{black} is the mean photon count from light scattered into the line of sight between the target (the little auk) and the observer (*T. inermis*), N_{space} is the mean photon count from background space-light, and X_{ch} is the number of false photons per integration time in a visual channel of *T. inermis*. All calculations and variables used for visual modeling, and their values are listed in Appendix B.

Bioluminescent communities in Kongsfjord were distributed at the measured 20m interval \pm 10m around each interval, and N_{bio} was calculated as the sum of bioluminescence originating from each taxon in these communities. Bioluminescence produced by a given taxon, $N_{\text{bio}_{\text{taxon}}}$, was determined from the number of point sources viewed by *T. inermis* and the mean point source emission (number of photons emitted in all directions) for that taxon (Appendix B). For each taxon, the number of point sources viewed by *T. inermis* was determined using measured abundances (ind. m^{-3}) from UBAT profiles to calculate nearest neighbor distance for randomly distributed individuals in 3-dimensional space (Clark and Evans 1979), and mean point source emission was calculated by integrating bioluminescent emissions measured in UBAT laboratory experiments and dividing by the duration of the emission.

Visual range was calculated using three different scenarios for the stimulated bioluminescent community in order to test whether variations in bioluminescent community composition altered visual performance. These included scenarios of: (1)

no bioluminescence throughout the entire water column; (2) the average depth-stratified Kongsfjord luminescent community as measured by UBAT, and (3) depth-stratified single-taxon luminescent assemblages based on measured abundances in Kongsfjord. In all visual models, the distance at which *T. inermis* could not discriminate between the little auk and the background was set at twice the wingspan of a little auk, 0.76m , or the point at which it subtended more than 28° of the visual field (see Nilsson et al. 2014).

2.3 Results

2.3.1 Physical properties and the underwater light field

During profiling at the study site, mean temperature ranged between -0.17 and 0.8 °C (\pm SE) throughout the water column, with the coldest temperatures above 30m (Fig. 2.2A). Mean salinity was less than 34.8 in the upper 27m, and mean σ_θ was between 27.85 and 27.93 for all depths below 1m. Downwelling irradiance modeled for measured atmospheric light on 25 January 2015 (Fig 2.2B) was 3.5×10^{-5} $\mu\text{mol photons m}^{-2} \text{s}^{-1}$ at the surface, decreasing to 5.5×10^{-13} $\mu\text{mol photons m}^{-2} \text{s}^{-1}$ at 99m. Photosynthetically active scalar irradiance, $E_{o,PAR}$, accounted for greater than 98% of total irradiance at the surface (3.64×10^{-5} $\mu\text{mol photons m}^{-3} \text{s}^{-1}$), while at 40m and deeper it accounted for 14% or less (Fig. 2.3). At 99m, $E_{o,PAR}$ contributed less than 1% to the total photon budget (6.8×10^{-13} $\mu\text{mol photons m}^{-3} \text{s}^{-1}$). Mean bioluminescence potential ranged between 2.4×10^{-8} and 1.4×10^{-7} (\pm SE) $\mu\text{mol photons m}^{-2} \text{s}^{-1}$ throughout the water column (Fig. 2.3), and bioluminescence potential contributed 85% or more of the total irradiance at 40m and deeper.

2.3.2 Bioluminescence in Kongsfjord

The number of bioluminescent emissions during profile stops increased with increasing depth to a maximum of 693 emissions m^{-3} at 80m (Fig. 2.4A), and there were significantly fewer emissions at 1m than at depths 40m and below (ANOVA, $F(6, 27)=5.661$, $P=0.001$). With the exception of the 60m depth interval, bioluminescence potential follows a similar pattern with a maximum of 6.2×10^{13} photons m^{-3} at 80m, but bioluminescence potential was not significantly different between depth intervals (Kruskal-Wallis test, $H_{25} = 13.027$, $P > 0.05$). Although also not significantly different between depth intervals (Kruskal-Wallis test, $H_{25} = 12.096$, $P=0.06$), the ratio of bioluminescence potential to emissions at shallower depths (1m and 20m) was about half of that at depths 40m and below. The greatest difference in both number of emissions and bioluminescence potential between consecutive depth intervals occurred between 20m and 40m (Fig. 2.4A).

Of the 17 taxa tested for the emission of bioluminescence using the UBAT, 7 taxa were bioluminescent and included in the library. These were copepods (*Metridia*), ctenophores (*Beroe* and *Mertensia*), dinoflagellates (*Protoperidinium*), krill (*Meganyctiphanes* and *Thysanoessa*), and ostracods (*Boroecia*) (Table 2.1). At each depth interval, these seven taxa varied in abundance (Table 2.2), with dinoflagellates comprising the greatest proportion of the bioluminescent community at the shallowest depths sampled (1m and 20m) and *Metridia* contributing the greatest proportion at 40m and deeper (Figure 2.4 B&C). Dinoflagellates decreased in their contribution with increasing depth, until leveling out at 15-20% of the community below 40m (Fig. 2.4C), while *Metridia* increased with increasing depth until 60m (Fig. 2.4B). *Metridia* were also the only taxa to vary significantly in abundance between depth intervals,

being significantly more abundant at 80m and 100m than they were at 1m or 20m (ANOVA, $F(6,27)=7.321$, $P<0.001$) (Table 2.2).

Fifteen to twenty percent of the bioluminescent community was composed of *Mertensia* above 80m, while it contributed 10-15% below 80m. (Fig. 2.4D). *Thysanoessa* and *Meganyctiphanes* were variable in their contribution to the bioluminescent community, but neither exceeded 6% of the community at any depth and both are lowest in their contribution in the upper 20m (Fig. 2.4E). *Boroecia* and *Beroe* comprised the smallest proportion of the community at all depths, with each species contributing less than 2%, and *Beroe* was only present in communities at 80m and deeper (Fig. 2.4F). At any depth, compound and unidentified emissions each constituted 16% or less of emissions (Fig. 2.4G). Multi-dimensional scaling indicated that all replicate samples at 40m and deeper were 80% similar, while replicates at 20m had an 80% similarity both to communities at 1m and to communities below 40m (Fig. 2.5).

During the four-minute pumping period at each depth interval, Shannon diversity increased throughout sampling, but depth-stratified communities reached maximum diversity at different rates (Fig. 2.6). Mean measured diversity, H' , reached a maximum at 60m, and was significantly higher at 40m and below than at 1m and 20m (t test, $t_{26} = -4.894$, $P<0.001$) (Table 2.3). Patterns of species evenness, J' , were similar to species diversity. In nonlinear regression models, the community at 40m was both the most diverse and the slowest to reach H'_{max} , while communities at 1m and 20m were the least diverse (Table 2.3).

2.3.3 Modeling the visual range of *Thysanoessa inermis*

In all models, the visual range of *T. inermis* was greatest at depths shallower than 11m. In this range downwelling light was intense enough for *T. inermis* to perceive the body of a little auk at distances greater than 11m, or greater than the available distance in the water column above it. In the absence of bioluminescence, the amount of light available for vision decreased exponentially with the attenuation of atmosphere-derived light, and the range at which *T. inermis* was able to perceive an approaching little auk decreased in an exponential manner as well (Fig. 2.7A, dotted line). With no bioluminescence, *T. inermis* could not perceive a little auk at depths below 45m.

However, the presence of the bioluminescent community affected the visual range of *T. inermis*. As downwelling light and stimulated bioluminescence approached each other in intensity in the top 25m, the visual range of *T. inermis* became increasingly short, until it could no longer distinguish between the little auk and the pelagic background (Fig. 2.7A, solid line). Between 25 and 27m depth visual range was short enough that the little auk occupied more than 28° of the visual field of *T. inermis*, and *T. inermis* could not perceive the little auk. Deeper than this, the visual range of *T. inermis* increased with increasing depth as downwelling light continued to decrease. Slight but abrupt changes in visual range occurred at depths where taxonomic abundances of bioluminescent plankton, and therefore the amount of stimulated bioluminescent light, were changed to reflect the community composition determined above.

When bioluminescence was modeled not as a community, but rather in separate cases assuming all emissions were from a single population of each of the three most abundant taxonomic groups in Kongsfjord, *Metridia* gave the longest visual

range to the target at depths where bioluminescent light exceeded downwelling light (Fig. 2.7B). Additionally, the point at which *T. inermis* could not distinguish the little auk from the pelagic background occurred at a shallower depth in *Metridia* models than in models of either dinoflagellate or ctenophore luminescence. At depths where stimulated bioluminescence was more intense than background light, the range given by the bioluminescent community model was greater than the range given by any scenario of single-taxon populations.

2.4 Discussion

The vertical distribution of pelagic plankton is influenced by a number of biological and physical processes including density stratification, turbulence, internal waves, and behaviorally-directed swimming (Gallager et al. 2004). As a result, planktonic bioluminescence and bioluminescent communities are often depth-stratified with distributions related to density discontinuities and changes in salinity and temperature (e.g. Widder et al. 1999, Moline et al. 2009). Planktonic communities in Kongsfjord are shaped by the advection and interaction of different water-mass types (Willis et al. 2006) as Atlantic water from the West Spitsbergen Current interacts with Arctic water and local glacial melt within the fjord (Cottier et al. 2005). During profiling in Kongsfjord, mean salinity, temperature and σ_θ measurements indicated an Arctic water mass in the top 27m, and local water below 27m (see Cottier et al. 2005 for water mass definitions) for the period of 21-24 January, 2014, with dinoflagellate-dominated bioluminescent communities above and *Metridia* dominated communities below this transition.

While transitioning water masses may facilitate changes in the bioluminescent community within this depth range, visual thresholds and diel vertical migrations

could also be factors shaping the distribution of bioluminescent taxa in Kongsfjord. Atmospheric irradiance in Kongsfjord at this time of year is dim ($1-1.5 \times 10^{-5}$ $\mu\text{mol photons m}^{-2} \text{ s}^{-1}$), yet zooplankton have been found to be able to perceive downwelling atmospheric light to 20-30m depth (Cohen et al. 2015) and to perform diel vertical migration between 30 and 60m during the winter in Kongsfjord (Berge et al. 2009). This combination of biological and physical dynamics within the range of 20m to 40m may create an ecotone for bioluminescent communities. Ecotones are transitional zones between patches of different and relatively homogenous ecological community types (van der Maal 1990) which often exhibit higher levels of biodiversity than surrounding patches (Risser 1995). Not only was mean Shannon diversity (H') significantly higher in communities at 40m and deeper than in shallow communities, but the community at 40m was distinct from other communities measured in the water column in that it required the longest time to reach maximum diversity during sampling with half-saturation values 30s longer than all other depths. In addition, multi-dimensional scaling indicated that replicate community samples at 20m had an 80% similarity both to communities at 1m and to communities below 40m, signifying that communities may begin to transition from dinoflagellate dominated communities to zooplankton dominated communities as shallow as 20m.

In autumn, Shannon indices of zooplankton diversity around Svalbard are generally low (median ranges: 1.4-2.1) because of the dominance of only a few taxa (e.g. *Calanus* spp. and *Oithona* spp.)(Dvoretzky and Dvoretzky 2014). In general, winter bioluminescent communities measured here were also dominated by a few taxa, and had a slightly lower diversity index, likely due to the limited number of bioluminescent taxa relative the 51 taxonomic groups of plankton previously found

around Svalbard in winter (Hirche and Kosobokova 2011). Arctic epipelagic bioluminescent communities have been found to be characterized by a high proportion of zooplankton species including: *Metridia* spp., *Thysanoessa* spp. *Oikopleura* spp. and *Boroecia* spp. (formerly *Conchoecia* sp.) (e.g. Buskey 1992), while in the current study bioluminescent communities in Kongsfjord were found to predominantly consist of *Metridia*, *Mertensia*, and dinoflagellates with lower abundances of *Thysanoessa*, *Meganyctiphanes*, *Beroe*, and *Boroecia*. In winter in Svalbard fjords zooplankton are unevenly distributed in the water column (Weslawski et al. 1991), but as seen here, are in lower concentrations in the uppermost 25m and increase below 50m (Hirche and Kosobokova 2011).

Similar to bioluminescence measurements made at marginal ice zones (Buskey 1992; Lapota et al. 1992), maximum bioluminescence in Kongsfjord during winter was related to relative abundance of phytoplankton and zooplankton, with lower bioluminescence potential in shallow communities that were dominated by dinoflagellates and higher bioluminescence potential in deeper communities dominated by *Metridia*. Both bioluminescence potential and the relative abundance of zooplankton peaked at 80m in Kongsfjord. Because dinoflagellate emissions are comparatively dim relative to zooplankton emissions, with a cumulative sum of bioluminescence, \sum_{\max} , at least an order of magnitude less than all zooplankton taxa sampled here, lower bioluminescence potential relative to the total number of emissions at 1m and 20m was due to the stronger presence of dinoflagellates at these depths. Additionally, *Mertensia* is the dimmest zooplankton taxon in the bioluminescent library, but contributes most to the zooplankton abundance in shallow waters. Previous flash kinetic work in Kongsfjord during the polar winter also found

dinoflagellates to be abundant in the top 30m and to account for a similar proportion (38%) of the bioluminescent community as they do here (Johnsen et al. 2014).

However, this is considerably lower than has been found in Norwegian fjords during summer, where dinoflagellates can account for up to 96% of bioluminescence in the upper 100m (Lapota et al. 1989), likely due to higher primary productivity being supported by brighter atmospheric irradiance at this time of year.

Because the underwater light field impacts the distribution and behavior of pelagic organisms, another contributing factor to the transition between communities between 20 and 40m may be that bioluminescence potential surpassed photosynthetically active scalar irradiance ($E_{o, PAR}$) and contributed a greater number of photons per cubic meter of water to the pelagic light budget for all depths 40m and deeper. In fact, within the range of 20m to 40m depth, bioluminescence potential transitions from contributing less than 3% of the pelagic photon budget to over 85%, and below 60m bioluminescence contributed over 98% of the pelagic photon budget. Through its influence on the visual range of a dominant micronekton, *T. inermis*, this transition from a light field dominated by atmosphere-derived photons to one consisting mostly of those from stimulated bioluminescence, was shown to be of particular importance to a winter trophic interaction in Kongsfjord.

Downwelling atmospheric light, measured at midday in Kongsfjord in 2015 and modeled for the upper 100m, was brightest at the surface, causing a diving little auk to appear as a dark silhouette against an ambient background to an upwards-looking *T. inermis*. In the absence of bioluminescence, *T. inermis* was able to distinguish this diving predator at depths up to 45m using only downwelling atmospheric light, and above 11m downwelling atmospheric light is intense enough

that the range of *T. inermis* is sufficient to perceive the little auk at the surface, regardless of the presence of bioluminescence. However, in surface waters, the danger of being consumed by visual predators (like diving birds) may outweigh the benefits of perceiving potential predators from far off (Hays 2003). Little auks are capable of diving to 35m, and in the summer in Kongsfjord have been found to dive between 8.5m and 12m to feed on *Calanus* copepods (Brown et al. 2012). In winter, however, the stomach contents of little auks have been found to contain high numbers of *T. inermis* rather than *Calanus* spp. (Berge et al. In Prep), indicating a preference for this bioluminescent prey during this time of the year.

The interaction of bioluminescence from communities in Kongsfjord stimulated around the body of the diving auk influences this trophic interaction by either reducing the contrast between the body of the little auk and background light in shallow water, or illuminating it at deeper depths. Due to the reduced contrast between the body of the little auk and the pelagic background between 25 and 27m, visual range was short enough that the little auk subtended more than 28° of the visual field of *T. inermis* [i.e. it occupied enough of the visual field that adjacent visual channels could not compare the target and the background (Nilsson et al. 2014)]. Many organisms in the pelagic zone use bioluminescence for counterillumination, a form of camouflage in which organisms emit light from ventral photophores to break up the shadow cast by their body (e.g. Harper and Case 1999). Below 11m, stimulated bioluminescence from the community acts in a similar manner and begins to camouflage the little auk's dark body from the krill, as atmosphere-derived light attenuates and begins to match the intensity of stimulated bioluminescence. At 25m, bioluminescence begins to appear as bright point sources against the progressively

dimmer background, but the counterillumination-like effect of stimulated bioluminescence continues until *T. inermis* is below 32m and the little auk may be viewed in reverse contrast as bioluminescent emissions illuminate its body (Nilsson et al. 2012). Here, bioluminescence stimulated by the wake of the diving little auk facilitated the discrimination of the auk from the pelagic background at a range 4.5m greater than is possible from the downwelling light field alone.

Evidence from the current and previous studies indicates that the 20m-40m range in Kongsfjord is of particular interest for biological activity during the Arctic winter. Within this region of the water column zooplankton perform diel vertical migration (Berge et al. 2009), the bioluminescent community transitions from a dinoflagellate to a *Metridia* dominated community, and key zooplankton reach their visual thresholds both for the perception of scalar irradiance (Cohen et al. 2015) and for the discrimination of potential predators. In part, this may be due to the dramatic shift in the pelagic light field (from one dominated by dim, downwelling atmospheric irradiance to one dominated by bioluminescent point sources). Bioluminescence transition zones, or areas where bioluminescence overtakes atmosphere-derived light in contribution to the pelagic photon budget, may therefore be of particular importance to understanding how bioluminescence structures planktonic communities.

In the context of the Arctic winter, as one moves northwards the polar night increases in duration and the sun increases in angle below the horizon (Berge et al. In Press.), meaning that atmosphere-derived light is dimmer for an extended period of time and shallower depths will experience lower levels of downwelling irradiance than they do in Kongsfjord. In these environments, bioluminescence will increase in relative contribution to the pelagic photon budget and bioluminescence transition

zones will occur shallower than they do in Kongsfjord. Moving further south from Kongsfjord, the light regime transitions from one that experiences a seasonal dark period to one that experiences a diel light cycle with daytime irradiance that is brighter than in Kongsfjord during the winter (Smith et al. 1989). In the Sargasso Sea, bioluminescence varies over a diel cycle and is greater during the night than during the day (Batchelder et al. 1992). In summer, bioluminescence potential in the upper 150m of the Sargasso Sea ranges from 5.2×10^{11} to 11×10^{11} photons m^{-3} with 800 to 1500 bioluminescent emissions m^{-2} (Batchelder et al. 1990), compared to measurements 10^{13} photons m^{-3} and 693 emissions m^{-3} in Kongsfjord. In ecosystems such as the Sargasso Sea, not only will bioluminescence transition zones occur deeper, but they are also likely to move throughout the water column on a diel cycle as the sun rises and sets and zooplankton perform diel vertical migrations. Targeting this vertically moving transition zone in the future may provide a better understanding of how light structures the planktonic community and affects visually mediated behaviors.

This study takes a first step in accounting for the depth-dependent dynamics of the bioluminescent community structure during the high Arctic winter and applies community-generated bioluminescence potential to pelagic trophic interactions through visual modeling. Further adapting visual models to incorporate the fine scale distribution and composition of bioluminescent communities, can demonstrate how aggregations and thin layers of bioluminescent plankton may affect vision in the pelagic environment. From the perspective of an individual *T. inermis* in Kongsfjord, the distribution and composition of the bioluminescent community can either help or hinder its ability to detect and react to potential predators by reducing or enhancing its visual range. As in the deep sea, bioluminescence potential in the Arctic winter likely

plays a disproportionate role in predator prey dynamics, due to the proportional differences between ambient light and bioluminescence potential compared to other areas of the globe. Finally, the transition between environments dominated by atmosphere-derived light to those dominated by bioluminescent light may have an important influence on ecosystem dynamics and visually-mediated behaviors.

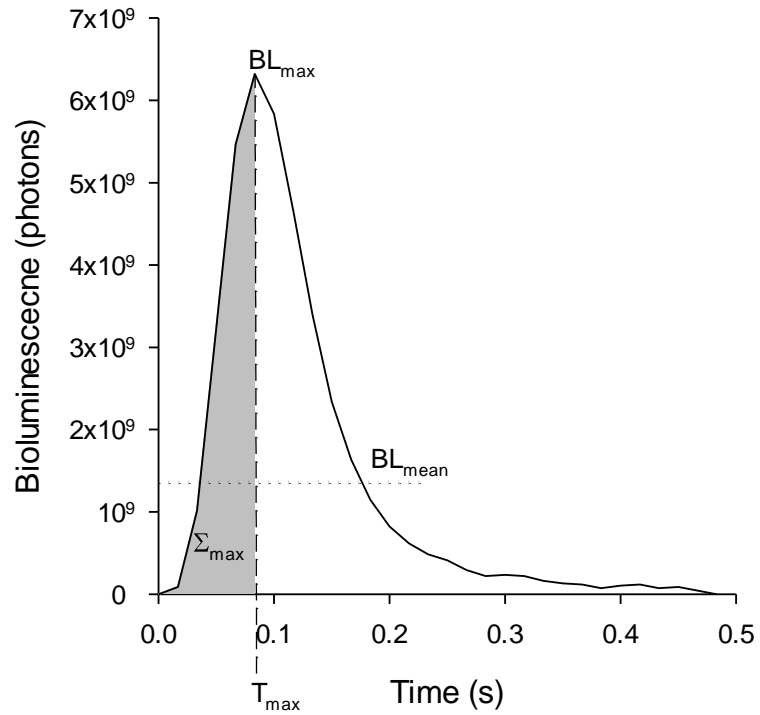


Figure 2.1: Flash kinetics for an emission from a laboratory-tested copepod *Metridia longa* showing parameters used to create taxonomic signatures for *in situ* identifications. Parameters include the maximum bioluminescence (BL_{max}), the average bioluminescence produced during the emission (BL_{mean}), the time until the emission reached maximum (T_{max}), and the cumulative sum of bioluminescence produced until the maximum (Σ_{max}).

Table 2.1: Flash kinetic parameter signatures (\pm SE) for taxa collected around Svalbard during 2012 and 2014. Sample size is in parentheses with each taxon. BL_{\max} , BL_{mean} , and Σ_{\max} are reported $\times 10^9$ photons s^{-1} , and T_{\max} is reported in seconds.

Taxon	Location	BL_{\max}	BL_{mean}	Σ_{\max}	T_{\max}
Dinoflagellates (n=7)	Rijpfjord, Billefjord	1.14 \pm 0.27	0.37 \pm 0.079	2.86 \pm 0.73	0.08 \pm 0.003
Gelatinous zooplankton					
<i>Beroe cucumis</i> (n=16)	Kongsfjord	200.05 \pm 48.43	65.45 \pm 18.16	3176.5 \pm 1557	0.52 \pm 0.078
<i>Mertensia ovum</i> (n=13)	Rijpfjord	2.05 \pm 0.41	0.66 \pm 0.13	17.21 \pm 4.51	0.34 \pm 0.066
Copepods					
<i>Metridia</i> spp. (n=13)	Kongsfjord	6.47 \pm 1.29	1.70 \pm 0.32	19.69 \pm 3.47	0.13 \pm 0.037
Krill					
<i>Meganyctiphanes norvegica</i> (n=6)	Kongsfjord	12.98 \pm 6.90	3.59 \pm 1.80	85.98 \pm 38.84	0.15 \pm 0.046
<i>Thysanoessa inermis</i> (n=18)	Kongsfjord	25.32 \pm 7.63	12.61 \pm 3.63	209.97 \pm 69.39	0.22 \pm 0.022
Ostracods					
<i>Boroecia</i> sp. (n=3)	Sea ice drift	76.65 \pm 39.11	22.24 \pm 11.10	323.27 \pm 146.82	0.34 \pm 0.19

Table 2.2: Mean abundances (individuals m⁻³, ±SE) of each taxon in the bioluminescence library for UBAT profiles (n=4) shown in Fig. 2.4. Abundances are calculated from the first 4 minutes (89.5 L) sampled.

Depth (m)	<i>B. cucumis</i>	<i>Boroecia</i> spp.	<i>Metridia</i> spp.	<i>M. norvegica</i>	<i>M. ovum</i>	<i>Thysanoessa</i> spp.	Dinoflagellates
1	0	5.59 ±5.59	71.63 ±10.86	2.79 ±2.79	72.08 ±18.62	0	119.56 ±6.98
20	0	2.79 ±2.79	114.50 ±28.98	2.79 ±2.79	92.16 ±25.54	5.59 ±3.22	122.88 ±27.36
40	0	0	164.77 ±12.38	16.76 ±9.67	108.91 ±18.45	30.72 ±5.35	114.50 ±11.51
60	0	5.59 ±3.22	226.21 ±15.38	22.34 ±11.17	106.12 ±16.12	19.55 ±9.54	108.91 ±16.04
80	2.79 ±2.79	5.59 ±3.22	231.79 ±37.15	25.13 ±2.79	103.33 ±12.38	22.34 ±10.18	122.88 ±13.68
100	5.59 ±3.22	8.38 ±5.35	242.96 ±17.88	22.34 ±7.99	58.65 ±9.54	30.72 ±5.35	100.54 ±12.07
120	2.79 ±2.79	8.38 ±5.35	192.69 ±31.10	22.34 ±11.17	75.40 ±12.38	27.93 ±11.17	114.50 ±21.08

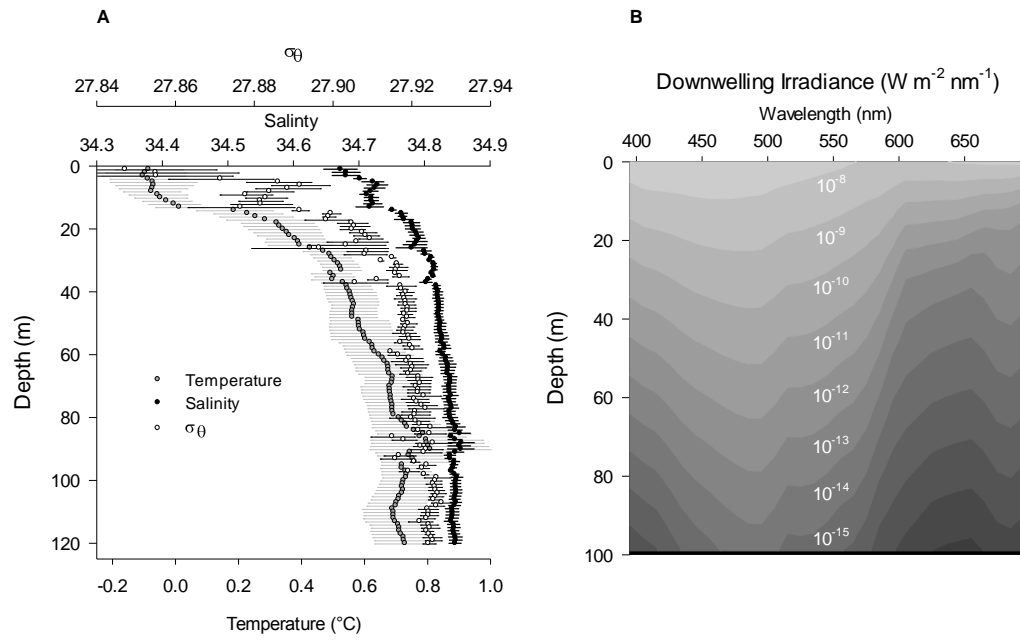


Figure 2.2: (A) Mean profiles ($n=3$) of salinity, temperature and σ_θ ($\pm\text{SE}$) taken by CTD (2014) concurrent with measurements of bioluminescence potential. (B) Downwelling spectral irradiance modelled in Kongsfjord for midday on 25 January 2015 as described in Methods (Section 2.2).

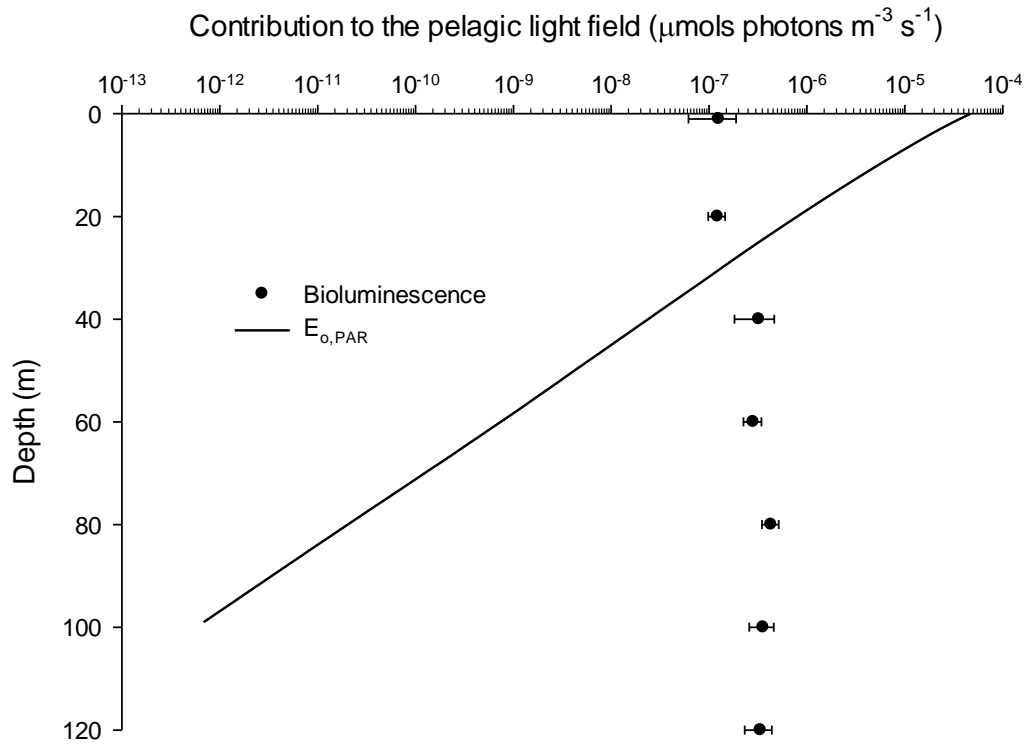


Figure 2.3: Distribution of photons from biological and atmospheric light sources as a function of depth in January in Kongsfjord. Photons from mean bioluminescence potential (\pm SE, black dots) measured at midday and midnight, and scalar irradiance between 400-700nm ($E_{o,PAR}$, solid line) modeled from diffuse atmospheric irradiance measured at approximately solar noon on 25 January 2015.

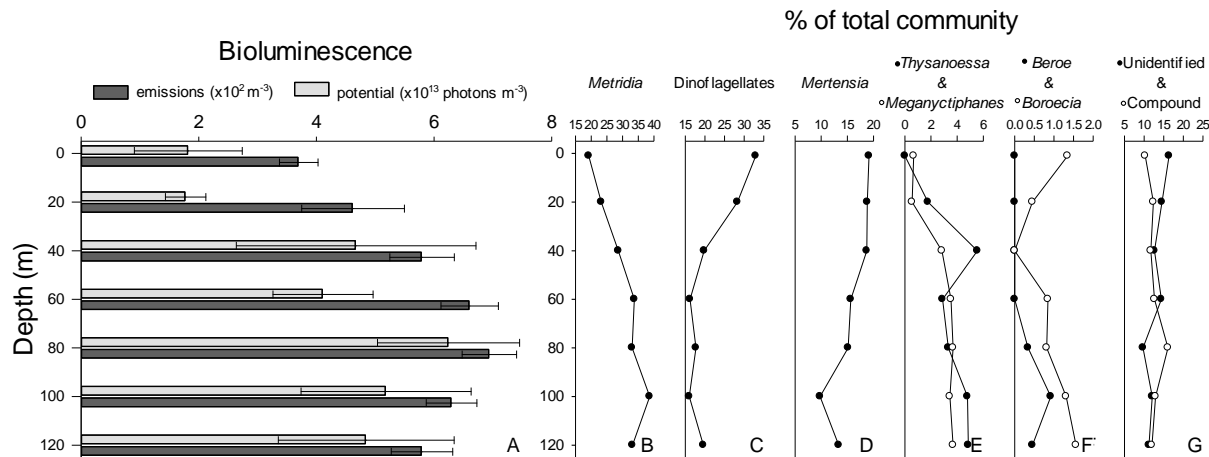


Figure 2.4 Bioluminescence profiles. (A) Profiles of mean bioluminescence potential (\pm SE, $n=4$) measured for 4 minutes at 20 m intervals. Profiles were taken in Kongsfjord (2014). Bioluminescence potential is represented as total number of emissions m^{-3} (dark bars) and in number of photons ($\times 10^{13} \text{ m}^{-3}$) produced (light bars). (B-G) Proportion of the bioluminescent community (as measured by number of emissions) comprised by each known bioluminescent taxonomic group and by unidentified individuals. Compound flashes which were not processed using the bioluminescence library are also included.

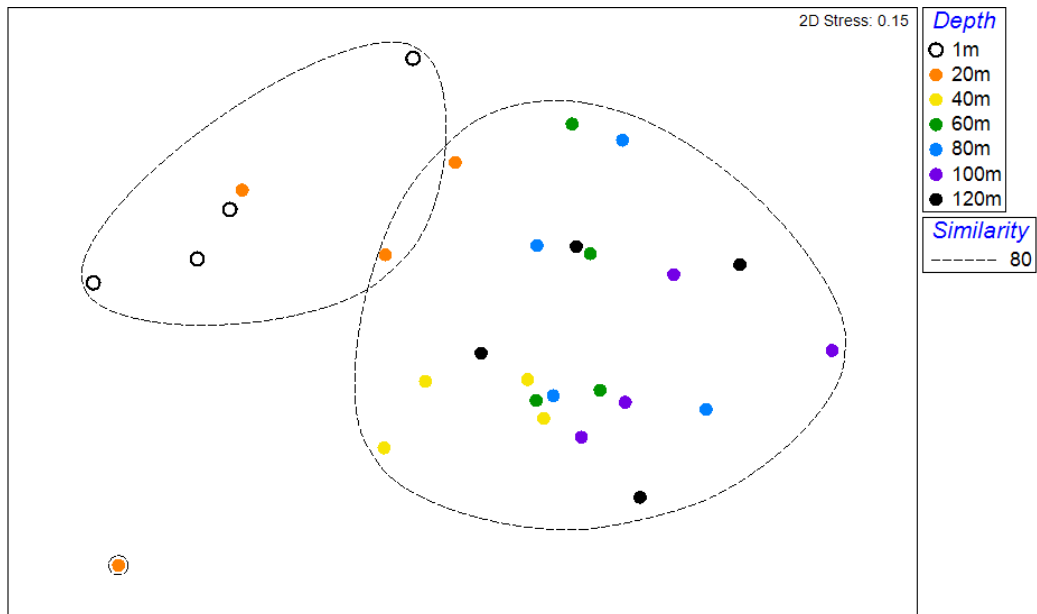


Figure 2.5: Multidimensional scaling of bioluminescent communities based on abundances (individuals m^{-3}) of 7 taxonomic groups (Table 2.2) for samples ($n=4$) at 20m depth intervals in UBAT profiles. Taxonomic abundances are square-root transformed and resemblance is plotted according to Bray-Curtis dissimilarity.

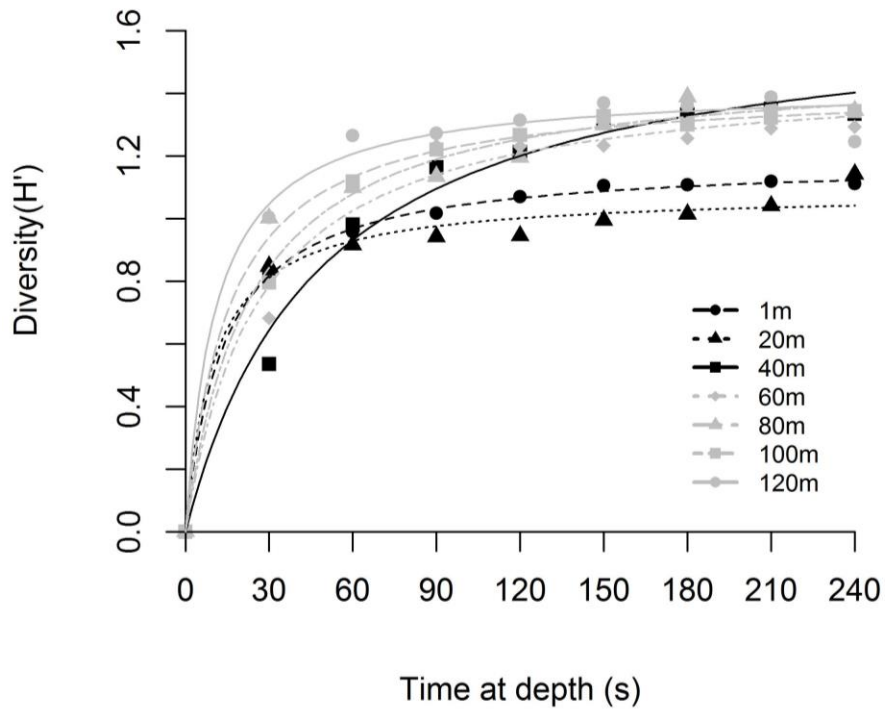


Figure 2.6: Mean ($n=4$) Shannon diversity at every 30s for each depth interval over the 4-minute (89.5 L) sampling period for profiles in Figure 2.4. Overlaid, is a nonlinear regression model for each depth. Grey symbols/lines represent communities at 60m and below, while dark symbols/lines represent communities at 40m and above.

Table 2.3: Maximum Shannon diversity (H'_{\max}) and the time (s) to reach $\frac{1}{2}$ of the maximum diversity (K) calculated from non-linear regression of Shannon diversity at every 30s during UBAT profiles (Fig. 2.6), and mean measured Shannon diversity (H') and Pielou's evenness (J') for the entire sampling period.

Depth (m)	Model Parameters		Measured	
	H'_{\max} (95% CI)	K (95% CI)	H'	J'
1	1.19(1.0-1.3)	14.1(0.16-28.1)	1.11	0.57
20	1.09(1.0-1.2)	11.6(5.2-18.1)	1.14	0.59
40	1.69(1.5-1.9)	57.7(33.4-82.0)	1.33	0.69
60	1.47(1.4-1.6)	27.2(15.6-38.7)	1.29	0.66
80	1.42(1.3-1.5)	14.8(7.9-21.8)	1.35	0.69
100	1.50(1.3-1.7)	23.0(4.2-41.8)	1.34	0.69
120	1.42(1.3-1.5)	12.0(5.3-18.6)	1.25	0.64

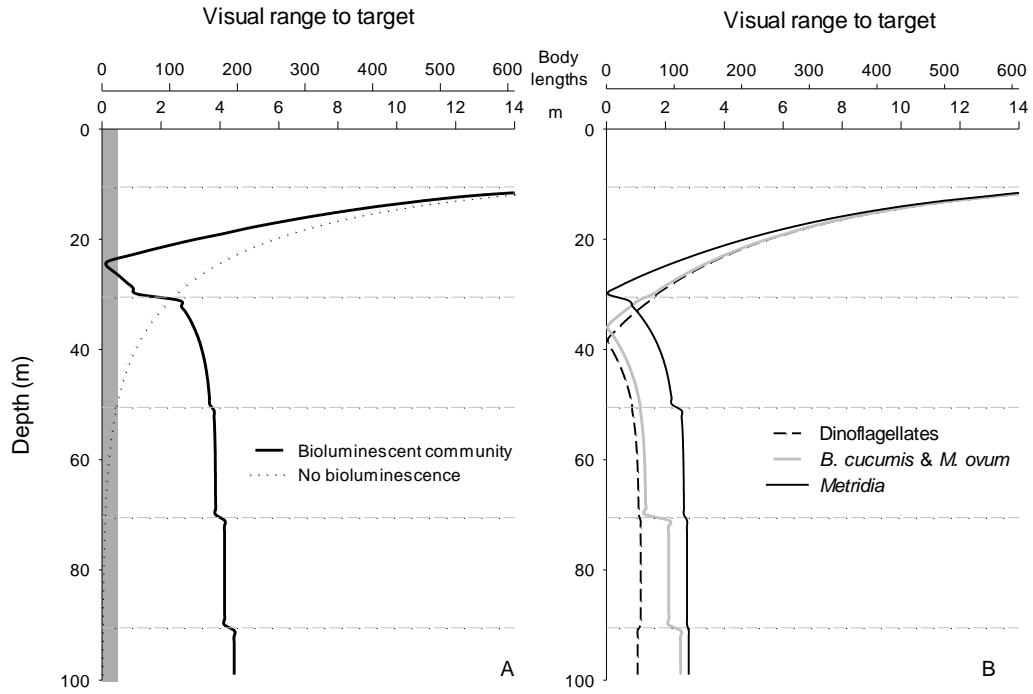


Figure 2.7 Visual range of an upward-looking *T. inermis* observing an approaching little auk (*Alle alle*) in light conditions shown in Figure 2.2B. (A) Visual range given the bioluminescent community determined from UBAT profiles in January 2014 (solid line) compared to no bioluminescence (dotted line). The shaded box represents the range (0.76m) within which the little auk subtended greater than 28° of the visual field of *T. inermis*. In this range, photoreceptors in the *T. inermis* eye could not simultaneously view both the little auk and the background, and therefore *T. inermis* could not discriminate the little auk. (B) Visual range given bioluminescence from single populations of each of the three most abundant taxonomic groups in Kongsfjord. Gray dashed lines in both panels represent depths at which the input community for the model was altered to reflect the community in Kongsfjord.

REFERENCES

- Batchelder H, Swift E, Van Keuren J. (1990) Pattern of planktonic bioluminescence in the northern Sargasso Sea: seasonal and vertical distribution. *Mar. Biol.* 104: 153-164.
- Batchelder H, Swift E, Van Keuren J. (1992) Diel patterns of planktonic bioluminescence in the northern Sargasso Sea. *Mar. Biol.* 113: 329-339.
- Båtnes AS, Miljeteig C, Berge J, Greenacre M, Johnsen G. (2013) Quantifying the light sensitivity of *Calanus* spp. during the polar night: potential for orchestrated migrations conducted by ambient light from the sun, moon, or aurora borealis? *Polar Biol.* 38: 51-65.
- Behrens K, Cox C (2013) *Seawatching: Eastern waterbirds in flight*. Houghton Mifflin Harcourt Publishing Company, New York.
- Berge J, Båtnes AS, Johnsen G, Blackwell SM, Moline MA (2012). Bioluminescence in the high Arctic during the polar night. *Mar Biol* 159: 231-237.
- Berge J, Cottier F, Darnis G, Falk-Petersen S, Gabrielsen T, Johnsen G, Last K, Leu E, Lønne OJ, Moline M, Nahrgang J, Renaud P, Seuthe L, Søreide J, Varpe Ø, Weslawski JM (In Press) In the dark: paradigms of Arctic ecosystems during polar night challenged by new understanding. *Prog. Oceanogr.*
- Berge B, Daase M, Renaud P, Ambrose Jr W, Darnis G, Last K, Leu E, Cohen J, Johnsen G, Moline M, Varpe Ø, Shunatova N, Balazy P, Morata N, Massabuau J, Falk-Petersen S, Kosobokova K, Hoppe C, Weslawski JM, Kuklinski P, Legeżyńska J, Nikishina D, Cusa M, Kedra M, Wlodarska-Kowalczyk M, Vogedes D, Camus L, Tran D, Michaud E, Gabrielsen TM, Cottier F, Granovitch A, Gonchar A, Krapp R, Callesen TA. (In Prep) Unexpected biological activity during the polar night offers new perspectives on a warming Arctic.
- Berge J, Cottier F, Last K, Varpe Ø, Leu E, Søreide J, Eiane K, Falk-Petersen S, Willis K, Nygård H, Vogedes D, Griffiths C, Johnsen G, Lorentzen D, Brierley A (2009) Diel vertical migration of Arctic zooplankton during the polar night. *Biol Lett*, 5:69-72.

- Bray, J. R., & Curtis, J. T. (1957). An ordination of the upland forest communities of southern Wisconsin. *Ecol.Monogr.* 27:326-349.
- Brown ZW, Welcker J, Harding AMA, Walkusz W, Karnovsky NJ. (2012) Divergent diving behavior during short and long trips of a bimodal forager, the little auk *Alle alle*. *J. Avian Biol.* 43:215-226.
- Buskey EJ. (1992). Epipelagic planktonic bioluminescence in the marginal ice-zone of the Greenland Sea. *Mar Biol*, 113: 689-698.
- Buskey ET, Swift E. (1985). Behavioral responses of oceanic zooplankton to simulated bioluminescence. *Biol. Bull.* 168: 263-275.
- Childress JJ, Cowles DL, Favuzzi JA, Mickel, TJ. (1990). Metabolic rates of benthic deep-sea decapod crustaceans decline with increasing depth primarily due to the decline in temperature. *Deep-Sea Res.* 37: 929-949.
- Clark PJ, Evans FC (1979) Generalization of a nearest neighbor measure of dispersion for use in k-dimensions. *Ecology* 60: 316-317.
- Cohen JH, Berge J, Moline MA, Sørensen AJ, Last K, Falk-Petersen S, Renaud P, Leu E, Grenvald J, Cottier F, Cronin H, Menze S, Norgren P, Varpe Ø, Daase M, Darnis G, Johnsen G (2015) Is ambient light during the high Arctic polar night sufficient to act as a visual cue for zooplankton? *Plos One* 10: e0126247. doi:10.1371/journal.pone.0126247
- Cottier F, Tverberg V, Inall M, Svendsen H, Nilsen F, Griffiths C. (2005) Water mass modification in an Arctic fjord through cross-shelf exchange: The seasonal hydrography of Kongsfjorden, Svalbard. *J. Geophys. Res-Oceans* 110.
- Cussatlegras AS, Geistdoerfer P, Prieur L. (2001). Planktonic bioluminescence measurements in the frontal zone of Almeria-Oran (Mediterranean Sea). *Oceanologica Acta.* 24: 239-250.
- Dawkins R, Krebs JR. (1979). Arms races between and within species. *P. Roy.Soc. Lond. B.Biol.* 205: 489-511.
- Dvoretzky VG, Dvoretzky AG. (2014). Biodiversity of zooplankton communities in the western Arctic seas. *Biologiya Morya (Vladivostok)*, 40(2), 108-112.

- Gallager SM, Yamazaki H, Davis, CS. (2004). Contribution of fine-scale vertical structure and swimming behavior to formation of plankton layers on Georges Bank. *Mar. Ecol. Prog. Ser.* 267:27-43.
- Gerrish, GA, Morin JG, Rivers TJ, Patrawala Z. (2009) Darkness as an ecological resource: the role of light in partitioning the nocturnal niche. *Oecologia*, 160: 525-536.
- Gitelzon II, Filimonov VS, Musonov VM. (1981). Bioluminescent glow of surface-water layer of the central Arctic in spring. *Doklady Akademii Nauk Sssr*, 256: 723-726.
- Haddock SHD, Case, JF. (1999) Bioluminescence spectra of shallow and deep-sea gelatinous zooplankton: ctenophores, medusae and siphonophores. *Mar Biol*, 133: 571-582.
- Haddock SH, Moline MA, Case, JF. (2010). Bioluminescence in the sea. *Ann Rev Mar Sci*, 2: 443-493.
- Haddock SHD, Dunn CW, Pugh PR, Schnitzler CE (2005) Bioluminescent and red-fluorescent lures in a deep-sea siphonophore. *Science*. 309: 263-263.
- Harper RD, Case JF. (1999). Disruptive counterillumination and its anti-predatory value in the plainfish midshipman *Porichthys notatus*. *Mar Biol*. 134: 529-540.
- Hays GC. (1995). Ontogenetic and seasonal variation in the diel vertical migration of the copepods *Metridia lucens* and *Metridia longa*. *Limnol. Oceanogr.* 40: 1461-1465.
- Hays GC. (2003). A review of the adaptive significance and ecosystem consequences of zooplankton diel vertical migrations. *Hydrobiologia*. 503: 163-170.
- Heger, A., Ieno, E. N., King, N. J., Morris, K. J., Bagley, P. M., & Priede, I. G. (2008). Deep-sea pelagic bioluminescence over the Mid-Atlantic Ridge. *Deep Sea Res. Pt. II*. 55: 126-136.
- Herren CM., Haddock SH, Johnson C, Orrico CM, Moline MA, Case JF. (2005) A multiplatform bathyphotometer for fine-scale, coastal bioluminescence research. *Limnol. Oceanog.: Methods*. 3: 247-262.
- Herring PJ. (1987) Systematic distribution of bioluminescence in living organisms. *J. Biolum. Chemilum.* 1:147-163.

- Herring PJ, Widder EA. 2004. Bioluminescence of deep-sea coronate medusae (Cnidaria: Scyphozoa). *Mar. Biol.* 146:39–51.
- Hirche HJ, Kosobokova KN. (2011). Winter studies on zooplankton in Arctic seas: the Storfjord (Svalbard) and adjacent ice-covered Barents Sea. *Mar Biol.* 158: 2359-2376.
- Johnsen G, Candeloro M, Berge J, Moline MA. (2014) Glowing in the dark: discriminating patterns of bioluminescence from different taxa during the Arctic polar night. *Polar Biol.* 37: 707-713.
- Johnsen, S. (2001). Hidden in plain sight: The ecology and physiology of organismal transparency. *Biol. Bull.*, 201: 301-318.
- Johnsen S. (2014). Hide and Seek in the Open Sea: Pelagic Camouflage and Visual Countermeasures. *Annu. Rev. Mar. Sci.* 6: 369-392.
- Jones BW, Nishiguchi MK. (2004). Counterillumination in the Hawaiian bobtail squid, *Euprymna scolopes* Berry (Mollusca : Cephalopoda). *Mar Biol.* 144:1151-1155.
- Kraft A, Berge J, Varpe Ø, Falk-Petersen S. (2012) Feeding in Arctic darkness: mid-winter diet of the pelagic amphipods *Themisto abyssorum* and *T. libellula*. *Mar Biol.* 160: 241-248.
- Kushnir VM, Tokarev YN, Williams R, Piontkovski SA, Evstigneev PV. (1997). Spatial heterogeneity of the bioluminescence field of the tropical Atlantic Ocean and its relationship with internal waves. *Mar. Ecol-Prog. Ser.* 160:1-11.
- Lampert W. 1993. Ultimate causes of diel vertical migration of zooplankton: new evidence for the predator avoidance hypothesis. *Arch. Hydrobiol. Beih. Ergeb. Limnol.* 39:79–88
- Land MF, Burton FA, Meyer-Rochow V. (1979) Optical geometry of euphausiids eyes. *J Comp Physiol* 130: 49-62.
- Land MF (1981) Optics and vision in invertebrates. In: *Handbook of sensory physiology*, vol. VII/6B (ed. H Autrum), 471–592. New York, NY: Springer.
- Lapota D, Geiger ML, Stiffey AV, Rosenberger DE, Young, DK. (1989) Correlations of planktonic bioluminescence with other oceanographic parameters from a Norwegian fjord. *Mar. Ecol. Press Ser.* 55: 217-227.

- Lapota D, Rosenberger DE, Lieberman SH. (1992). Planktonic bioluminescence in the pack ice and the marginal ice zone of the Beaufort Sea. *Mar Biol*, 112(4), 665-675.
- Latz MI, Rohr J. (2013). Bathypotometer bioluminescence potential measurements: A framework for characterizing flow agitators and predicting flow-stimulated bioluminescence intensity. *Cont. Shelf Res.* 61-62: 71-84.
- Li YQ, Swift E, Buskey EJ. (1996). Photoinhibition of mechanically stimuable bioluminescence in the heterotrophic dinoflagellate *Protoperidinium depressum* (Pyrrophyta). *J. Phycol.* 32: 974-982.
- Mensing AF, Case JF. (1992) Dinoflagellate luminescence increases susceptibility of zooplankton to teleost predation. *Mar. Biol.* 112: 207–10.
- Moline MA, Blackwell SM, Case JF, Haddock SHD, Herren CM, Orrico CM, Terrill E. (2009) Bioluminescence to reveal structure and interaction of coastal planktonic communities. *Deep Sea Res. Pt. II:* 56: 232-245.
- Nilsson DE, Warrant EJ, Johnsen S, Hanlon R, Shashar N. (2012) A unique advantage for giant eyes in giant squid. *Curr. Biol.* 22: 683-688.
- Nilsson DE, Warrant E, Johnsen S. (2014) Computational visual ecology in the pelagic realm. *Philos. Trans. R. Soc. Lond. B. Biol. Sci.* 369: 20130038.
- Partridge JC, Douglas RH (1995) Far-red sensitivity of dragon fish. *Nature* 375: 21-22.
- Pielou, E. C. (1966). Measurements of diversity in different types of biological collections. *J.Theor. Biol.* 13: 131.
- Piontkovski SA, Tokarev YN, Bitutov EP, Williams R, Kiefer DA. (1997) The bioluminescent field of the Atlantic Ocean. *Mar. Ecol-Prog. Ser* 156:33-41.
- Risser PG. (1995) The status of the science examining ecotones-a dynamic aspect of landscape is the area of steep gradients between more homogeneous vegetation associations. *Bioscience.* 45: 318-325.
- Rivers TJ, Morin JG. (2008). Complex sexual courtship displays by luminescent male marine ostracods. *J. Exp. Biol.* 211: 2252-2262.
- Robison BH. (1992). Bioluminescence in the benthopelagic holothurian *Enypiastes-eximia*. *J. Mar. Biol. Assoc. UK.* 72: 463-472.

- Robison BH, Reisenbichler KR, Hunt JC, Haddock SHD. (2003) Light production by the arm tips of the deep-sea cephalopod *Vampyroteuthis infernalis*. *Biol. Bull.* 205:102–109.
- Shannon CE. (1948). A mathematical theory of communication. *AT&T Tech J.* 27: 379-423.
- Smith RC, Marra J, Perry MJ, Baker KS, Swift E, Buskey E, Kiefer DA. (1989) Estimation of a photon budget for the upper ocean in the Sargasso Sea. *Limnol Oceanog.* 34:1673-1693.
- Sullivan JM, Swift E. (1994). Photoinhibition of mechanically stimuable bioluminescence in the autotrophic dinoflagellate *Ceratium-fusus* (Pyrrophyta). *J. Phycol.* 30: 627-633.
- Vacquié-Garcia J, Royer F, Dragon AC, Viviant M, Bailleul F, Guinet C (2012) Foraging in the darkness of the Southern Ocean: influence of bioluminescence on a deep diving predator. *PLoS ONE* 7: e43565
- Van der Maarl E. (1990) Ecotones and ecoclines are different. *J. Veg. Sci.* 1: 135-138.
- Warrant E. (2004). Vision in the dimmest habitats on Earth. *J.Comp. Physiol. A.*190: 765-789.
- Warrant EJ. (1999) Seeing better at night: life style, eye design and the optimum strategy of spatial and temporal summation. *Vision Res.* 39:1611–1630.
- Warrant EJ, Locket NA (2004) Vision in the deep sea. *Biol. Rev. Camb. Philos. Soc.* 79: 671–712.
- Webster CN, Varpe O, Falk-Petersen S, Berge J, Stubner E, Brierley A. (2015) Moonlit swimming: vertical distributions of macrozooplankton and nekton during the polar night. *Polar Biol.* 38: 75-85.
- Weslawski JM, Kwasniewski S, Wiktor J. (1991) Winter in a Svalbard fjord ecosystem. *Arctic* 44: 115-123.
- Widder EA, Johnsen S. (2000) 3D spatial patterns of bioluminescent plankton: a map of the 'minefield'. *J. Plankton Res.* 22: 409-420.
- Widder EA., Johnsen S., Bernstein SA, Case JF, Neilson DJ. (1999) Thin layers of bioluminescent copepods found at density discontinuities in the water column. *Mar. Biol.* 134: 429-437.

- Widder EA, Case JF, Bernstein SA, MacIntyre S, Lowenstine MR, Bowlby MR, Cook DP. (1993) A new large volume bioluminescence bathyphotometer with defined turbulence excitation. *Deep Sea Res. Pt. I*: 40: 607-627.
- Widder EA (2002) Bioluminescence and the pelagic visual environment. *Mar. Freshwat. Behav. Physiol.* 35: 1–26.
- Widder EA. (2010) Bioluminescence in the ocean: origins of biological, chemical, and ecological diversity. *Science*. 328:704-708.
- Willis K, Cottier F, Kwasniewski S, Wold A, Falk-Petersen S. (2006) The influence of advection on zooplankton community composition in an Arctic fjord (Kongsfjorden, Svalbard). *J. of Marine Syst.* 61: 39-54.
- Wilson T, Hastings JW. (1998). Bioluminescence. *Annu. Rev. Cell Dev. Bi.* 14: 197-230.
- Zylinski S, Johnsen S. (2011). Mesopelagic cephalopods switch between transparency and pigmentation to optimize camouflage in the deep. *Cur. Biol.* 21: 1937-1941.

Appendix A

DEVELOPMENT OF *IN SITU* IDENTIFICATION METHOD

In order to further develop a method for identifying bioluminescent organisms in Kongsfjord from emissions in a UBAT, flash kinetics from laboratory-tested individuals were used to assess the accuracy of identification and to develop an iterative process for identification. Plankton were collected in Kongsfjord from 70m using a 180µm plankton net directly after UBAT profiles and were tested for bioluminescence no more than 24 hours after collection. Flash kinetics used to test the identification method were the same as those used to develop taxon-specific flash kinetic signatures.

First, flash kinetics from individuals of a given taxon were compared against the signature developed for that taxon (See Table 2.1 for taxon-specific signatures), using the error calculation from Johnsen et al. (2014). Briefly, the error for each parameter (φ) was calculated to find the distance between the parameter for the taxon signature and the laboratory emission:

(Eq. A.1)

$$\varphi = \frac{|Parameter_{emission} - Paramater_{taxon\ signature}|}{\| Parameter_{emission}, Paramater_{taxon\ signature} \|_{\infty}}$$

The error for each of the parameters was summed and divided by the number of parameters (4) to calculate the cumulative error ($\bar{\varphi}$) for each laboratory emission.

(Eq. A.2)

$$\bar{\varphi} = \frac{(\varphi_{BLmax} + \varphi_{BLmean} + \varphi_{\Sigma max} + \varphi_{Tmax})}{4}$$

Finally, mean $\bar{\varphi}$ was found for all laboratory emissions of a given taxon to develop Φ_{Taxon} . The standard deviation of Φ_{Taxon} ($\sigma\Phi_{Taxon}$) was also found for every taxon in the library.

Eq. (A.3)

$$\Phi_{Taxon} = \frac{\sum_{i=1}^n \bar{\varphi}_{Taxon_i}}{n}$$

Eq. (A.4)

$$\sigma\Phi_{Taxon} = \sqrt{\frac{\sum(\bar{\varphi}_{Taxon_i} - \Phi_{Taxon})^2}{n - 1}}$$

To determine the most accurate method for *in situ* identifications, laboratory-tested individuals were first identified as the taxon for which they had the smallest $\bar{\varphi}$, and then using an iterative method that implemented an identification threshold for each taxon. Because the bioluminescence library was comprised of only 7 taxonomic groups and was not a complete listing of bioluminescent taxa in Kongsfjord (e.g. appendicularians are absent from the library), a threshold for identification was implemented to account for unidentifiable individuals belonging to taxa that are not included in the library. The threshold for identification as a given taxon was set as $\Phi_{Taxon} + \sigma\Phi_{Taxon}$ (Table A.1), and if $\bar{\varphi}$ for an emission was below the taxon-specific threshold it was identified as that taxon. Multiple orders of identification were tested for the iterative method and the order which produced the largest percentage of correct identifications (Table A.2) was used for the identification of *in situ* emissions.

Table A.1: Mean cumulative error (Φ) and standard deviation of that error ($\sigma\Phi$) used to create a taxon-specific threshold value for $\bar{\varphi}$, the cumulative error between an *in situ* emission and a taxonomic signature.

Taxon	Φ	$\sigma\Phi$	$\bar{\varphi}$ Threshold
<i>Beroe</i>	0.46	0.06	0.53
<i>Boroecia</i>	0.53	0.16	0.69
Dinoflagellates	0.30	0.06	0.36
<i>Meganyctiphanes</i>	0.57	0.08	0.64
<i>Mertensia</i>	0.48	0.05	0.52
<i>Metridia</i>	0.46	0.04	0.50
<i>Thysanoessa</i>	0.55	0.05	0.61

Table A.2: Percentage of correct identifications for each taxon tested in the laboratory, using different sequences of iterative identification. “% within threshold” represents the percentage of individuals from the laboratory dataset with a $\bar{\varphi}$ which fell within the identification threshold, and were able to be identified using this method. Order 1 was used for *in situ* identifications in Kongsfjord.

Taxon	% within threshold	Order 1 ^a	Order 2 ^b	Order 3 ^c	Order 4 ^d
<i>Beroe</i>	56	56	56	56	56
<i>Boroecia</i>	67	67	0	67	67
Dinoflagellates	57	57	57	57	57
<i>Meganyctiphanes</i>	67	17	0	17	17
<i>Mertensia</i>	55	50	18	55	23
<i>Metridia</i>	39	39	39	17	39
<i>Thysanoessa</i>	50	6	50	6	6

a. Order 1: *Beroe*, *Boroecia*, *Metridia*, *Mertensia*, *Thysanoessa*, *Meganyctiphanes*, dinoflagellates

b. Order 2: *Beroe*, *Metridia*, *Thysanoessa*, *Meganyctiphanes*, *Mertensia*, *Boroecia*, dinoflagellates

c. Order 3: *Beroe*, *Mertensia*, *Metridia*, *Boroecia*, *Thysanoessa*, *Meganyctiphanes*, dinoflagellates

d. Order 4: *Beroe*, *Metridia*, *Mertensia*, *Boroecia*, *Thysanoessa*, *Meganyctiphanes*, dinoflagellates

Appendix B

VISUAL MODELS

B.1 Model Parameters

Visual range was determined for the detection of an extended black target triggering bioluminescence using calculations customized from Nilsson et al. (2014) for *T. inermis* in Kongsfjord viewing a little auk, *Alle alle*, against downwelling space-light (Table B.1), and was found by generalized reduced gradient (GRG) nonlinear optimization of the following equation:

Eq. (B.1)

$$|N_{\text{bio}} + N_{\text{black}} + N_{\text{space}}| = R \sqrt{N_{\text{bio}} + N_{\text{black}} + N_{\text{space}} + 2X_{\text{ch}}}$$

N_{bio} , or the photon count originating from bioluminescent point sources, was taken to be the sum of bioluminescence produced from every taxon in the bioluminescent community, and $N_{\text{bio}_{\text{taxon}}}$, the photon count originating from each bioluminescent taxon, was calculated according to Nilsson et al. (2014) using taxon-specific values for point source emission, E (Table B.2), and point source density, x .

Eq. (B.2)

$$N_{\text{bio}} = \Sigma N_{\text{bio}_{\text{taxon}}}$$

Eq. (B.3)

$$N_{\text{bio}_{\text{taxon}}} = P_{\text{taxon}} \left(\frac{E_{\text{taxon}} A^2}{16r^2} \right) e^{-\alpha * r} q \Delta t$$

Taxon-specific point source emissions were calculated by integrating emissions measured in the UBAT under laboratory conditions and dividing by the duration of the emission in seconds. Taxon-specific point source density, x , was calculated in 20m depth bins as nearest neighbor distance for randomly distributed individuals in 3-dimensional space (Clark and Evans 1979) using average measured abundances, ρ (ind. m⁻³), in Kongsfjord.

Eq. (B.4)

$$x = \frac{0.55397}{\rho^{1/3}}$$

The values used for variables in visual range calculations were determined from literature values, models of downwelling atmospheric light, and measurements made in Kongsfjord during January 2014 and 2015 (Table B.3) as described below.

B.1.1 *Thysanoessa inermis* eye morphology

Values for focal length, f , and photoreceptor diameter, d , were required to parameterize visual models for *Thysanoessa inermis*. Therefore, in January 2014 four dark-adapted *T. inermis* (mean body length=24.5mm ±1.4) were preserved in 4% formaldehyde and kept in darkness for later determination of eye morphology. The heads of these individuals were dehydrated in a graded ethanol series and embedded in LR White resin. Tissue was sectioned at 2 μm on a Sorval MT2-B ultramicrotome, stained with Toluidine Blue and Basic Fuchsin (EMS Epoxy tissue Stain), and mounted on slides with Permout (Fisher Chemical). Using a compound microscope, rhabdom diameter was measured for eight reticular cells in each individual (Fig. B.1). The average rhabdom diameter (d) of 9.6 μm (± 1.8 SD) was used in all models. For

the superposition compound eyes of krill, focal length (f) is equivalent to the distance from the center of the rhabdoms to the center of curvature of the eye, or nodal point (Land et al. 1979) (Fig. B.1), which was measured to be $213 \mu\text{m}$ (± 43 , SD) and was used in all models.

B.1.2 *Thysanoessa inermis* eye physiology

Critical flicker fusion frequency of *T. inermis* was used for integration time, Δt , in visual models, and *T. inermis* spectral sensitivity was used to weight downwelling space light (described below) to produce “krill utilized photons” (Cohen et al. 2015) at 1m depth intervals over the water column. Integrated “krill utilized photons”, or the amount of downwelling radiance available to *T. inermis* due its spectral sensitivity, were used for the I_{space} parameter in models.

Via extracellular electroretinogram recording, spectral sensitivity of *T. inermis* collected in Kongsfjord was determined in January 2014 from locations where bioluminescence measurements were made (Cohen et al. 2015), and critical flicker fusion frequency was found during January 2015 with animals from the same general location (J. Cohen, unpublished data). For both measurements, under dim red light *T. inermis* were attached dorsally to a plastic post using cyanoacrylate glue and suspended in a recording chamber with cold seawater ($1-5^{\circ}\text{C}$). Electroretinograms in response to a monochromatic light stimulus at the position of the eye were recorded using a tungsten microelectrode inserted subcorneally. Spectral sensitivity was determined by adjusting the irradiance of the stimulus at each test wavelength until a criterion response was reached, and *T. inermis* was found to be most sensitive at 492nm (Cohen et al. 2015). Critical flicker fusion frequency of *T. inermis* was determined by the frequency at which the eye could no longer respond to individual

flashes of a flickering light stimulus at the wavelength of maximum sensitivity as described in Cohen and Frank (2006). This value was 20 Hz for *T. inermis* kept at 1°C (J. Cohen, unpublished data), which gave an integration time, Δt , of 0.05s.

B.1.3 Underwater Light Field in Kongsfjord

For every output depth in visual models, a value for radiance of background space-light, I_{space} , the attenuation coefficient of background radiance, κ , and the beam attenuation coefficient of seawater, α , were required to calculate visual range. The beam attenuation coefficient of seawater was set as the average “c” value at 488nm, 0.147 m^{-1} , from an AC-9 (WetLabs, USA) profile taken to 100m in Kongsfjord in January 2015.

I_{space} and κ were both calculated using the radiative transfer software Hydrolight 5.2 RTE model (Mobley & Sundman 2001). Diffuse spectral irradiance was measured using a QE Pro spectrometer (Ocean Optics, FL, USA) that received 180° of diffuse skylight reflected from a Spectralon plate in Ny Ålesund at midday on January 25th, 2015 (J. Cohen, unpublished data). This was used as input to model the underwater light field throughout the water column for moonlit, clear conditions with Raman scattering and Chlorophyll-*a* fluorescence of $0.06 \mu\text{g L}^{-1}$ over the whole water column. Inherent optical properties in Kongsfjord necessary for radiative transfer modeling were measured in the AC-9 profile described above. Downwelling radiance from 395nm to 695nm was modeled in 5nm increments for every meter to 99m. These values were weighted based on the spectral sensitivity of *T. inermis*, and integrated using a trapezoidal integration from 395 to 655nm to generate a value for I_{space} , or the radiance of background space light at the position of the eye, for every meter to 99m. The attenuation coefficient of background radiance, κ , was set as the attenuation value

for downwelling radiance at 495nm calculated by Hydrolight. Diffuse skylight inputs and AC-9 values were similar to those measured at the time of UBAT profiles in January 2014.

B.2 ADDITIONAL MODEL RESULTS

Modeling perception using depth stratification of bioluminescent communities captures nuances in the bioluminescent light field caused by variation in the composition of the bioluminescent community and maximizes the range at which prey are able perceive potential predators. For understanding visually-mediated trophic interactions in the pelagic realm, incorporating bioluminescent community dynamics, rather than using assumptions of single-taxon distributions, may reveal different implications for population dynamics due to effects on visual ranges. Therefore, in order to compare model results from abundances of bioluminescent plankton and point source emissions measured in Kongsfjord to previous models using theoretical values, additional models were created for the inherent optical properties and modeled downwelling light in Kongsfjord using theoretical abundances and point source emission for single-taxon assemblages of dinoflagellates, gelatinous zooplankton, and copepods. With the exception of values for nearest neighbor distances, x , and point source emissions, E , models were as described in Chapter 2. Taxonomic abundances were assumed to be constant for every depth and community dynamics were not considered. For copepods (Fig. B.2, black solid line) a constant nearest neighbor distance of 0.2m and point source emission of 10^{10} photons s^{-1} was used to calculate N_{bio} at every depth (Widder and Johnsen 2000); for gelatinous zooplankton (Fig. B.2, gray line) nearest neighbor distance was 0.6m and point source emission was 10^{11} photons s^{-1} (Widder and Johnsen 2000), and for dinoflagellates (Fig. B.2, black dashed

line) nearest neighbor distance was 0.02m and point source emission was 10^{11} photons s^{-1} (Widder 2002).

The use of theoretical values, rather than measured values for nearest neighbor distance and point source emission, altered the range at which the target was perceived. When considering gelatinous zooplankton and copepods, models showed comparable results to those of measured abundances and point source emissions of *Metridia* assemblages and *Beroe* and *Mertensia* assemblages in Kongsfjord during this time of year. For dinoflagellates, however, theoretical values for point source emission and nearest neighbor distances (Widder 2002) were higher than those measured in Kongsfjord, and models estimated the visual range of *T. inermis* to be 25 to 30m greater than models using measurements from Kongsfjord. Additionally, if constant, theoretical values are applied for the whole water column, models failed to capture changes in visual range caused by variance in taxon abundances.

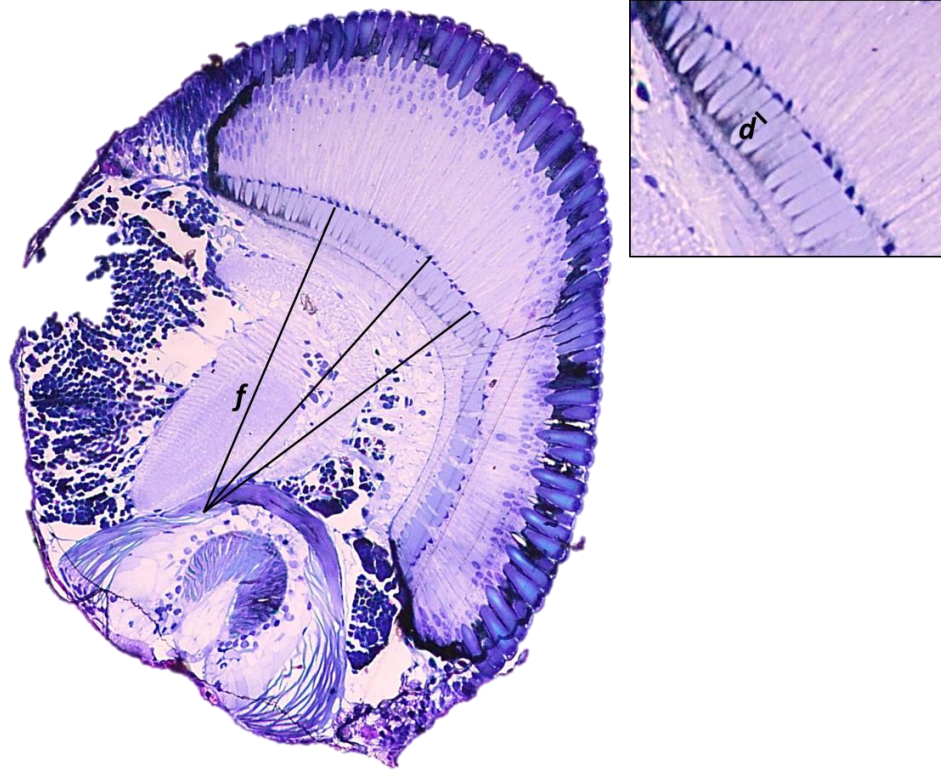


Figure B.1: Sagittal section of a *T. inermis* eye showing focal length, f , and photoreceptor diameter, d . This individual was collected in Kongsfjord during January 2015.

Table B.1: A list of component equations for visual models of the detection of an extended black target triggering bioluminescence and a description of their purposes. All equations are from Nilsson et al. (2014). Variable definitions and their values are listed in Table B.3.

Description	Equation
N_{space} ; the mean photon count originating from background space light	$0.617A^2\left(\frac{T}{r}\right)^2q\Delta t * I_{space}$
N_{black} ; the mean photon count originating from light scattered into the line of sight	$0.617A^2\left(\frac{T}{r}\right)^2q\Delta t * I_{space}(1 - e^{-(\kappa-\alpha)r})$
N_{bio} ; the mean photon count originating from all bioluminescent sources	$\Sigma N_{bio_{taxon}}$
$N_{bio_{taxon}}$; the mean photon count originating from a single bioluminescent taxon	$P_{taxon} \left(\frac{E_{taxon}A^2}{16r^2} \right) e^{-\alpha*r} q\Delta t$
x ; the average distance between bioluminescent point sources across an extended object	$\frac{0.55397}{\rho^{1/3}}$
X_{ch} ; the number of false photons per integration time	$\left(\frac{Tf}{rd}\right)^2 X\Delta t$
P_{taxon} ; total number of point sources from each taxon in the bioluminescent community viewed by the target pixel	$\frac{\pi T^3}{2.86x^3}$

Table B.2: Taxon-specific E-values for each of the seven taxa in the bioluminescence library.

Taxon	E_{taxon}
<i>Beroe</i>	4.51×10^{10}
<i>Boroecia</i>	1.30×10^{10}
Dinoflagellates	4.13×10^8
<i>Metridia</i>	1.59×10^9
<i>Mertensia</i>	6.50×10^8
<i>Meganyctiphanes</i>	3.33×10^9
<i>Thysanoessa</i>	1.07×10^{10}

Table B.3: Variables used in visual models and their values. Variables are from Nilsson et al. (2014); ρ is for calculations of nearest neighbor distances from Clark and Evans 1979 (see above).

Variable	Value	Units	Source
R : reliability coefficient	1.96		set for a 95% confidence interval (Nilsson et al. 2014; from Land 1981)
T : width of target	0.381	m	Wingspan of a little auk (Behrens and Cox 2013)
f : focal length	0.000213	m	Measured from sagittal sections of <i>T. inermis</i> eyes
r : range to target	--	m	Found for every output depth using GRG nonlinear optimization of Eq. B.1
d : photoreceptor diameter	0.0000096	m	Measured from sagittal sections of <i>T. inermis</i> eyes
X : dark noise per photoreceptor	0.000028	photons s ⁻¹	Nilsson et al. 2014, value from Warrant and Lockett (2004)
Δt : integration time	0.05	s	Critical flicker fusion frequency from electrophysiology of <i>T. inermis</i> in January 2015 (Cohen, unpubl. data)
A : pupil diameter	0.000549	m	Based on ½ of the eye diameter (Land et al. 1979)
q : detection efficiency	0.36		Nilsson et al. 2014; value from Warrant 1999
I_{space} : radiance of background space light in the direction of view	--	photons m ⁻² s ⁻¹ sr ⁻¹	Modeled in Hydrolight (5.2 RTE), weighted by the spectral sensitivity of <i>T. inermis</i> (Cohen et al. 2015)
κ : attenuation coefficient of background radiance	0.166	m ⁻¹	Modeled at 495nm using Hydrolight (5.2 RTE)
α : beam attenuation coefficient of seawater	0.147	m ⁻¹	Average “c” value at 488nm from an AC-9 profile in Kongsfjord in January 2015
ρ : taxon abundance	--	Individuals m ⁻³	Measured in UBAT profiles for each taxon and variable by taxon and depth bin

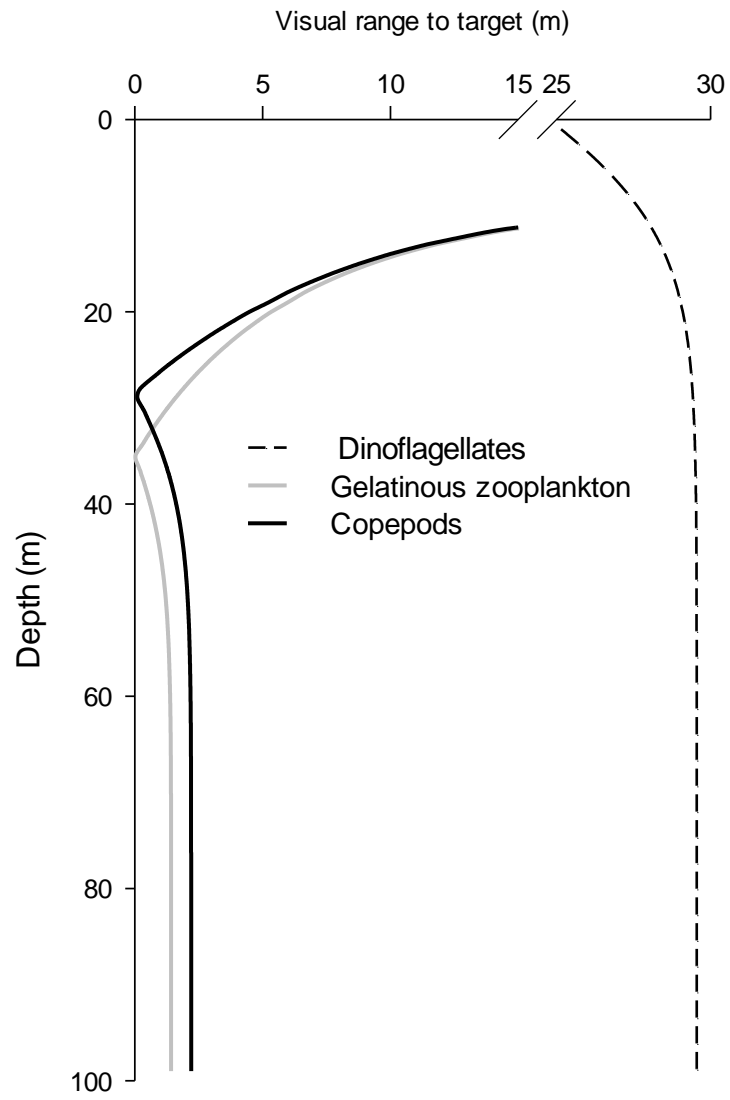


Figure B.2: Visual range of *T. inermis*, found using theoretical values of nearest neighbor distance and point source emissions for common taxonomic groups in Kongsfjord.